On the Deep Western Boundary Current Separation and Anticyclone Genesis off Northeast Brazil

Felipe Vilela-Silva[a*], Ilson C. A. Silveira[a], Dante C. Napolitano[b†], Pedro W. M. Souza-Neto[a], Tiago C. Biló[c], Avijit Gangopadhyay[d]

[a]Instituto Oceanográfico, Universidade de São Paulo, São Paulo, SP, BR
[b]Université de Toulouse, LEGOS (CNES/CNRS/IRD/UPS), Toulouse, OCC, FR
[c]Scripps Institution of Oceanography, University of California San Diego. La Jolla, CA, USA
[d]School for Marine Science and Technology, University of Massachusetts Dartmouth, New Bedford, MA, USA

Key Points:

- Part of the DWBC separates inertially off the continental slope while crossing the Pernambuco Plateau at 8°S.
- The DWBC separation plays a crucial role in the formation of the DWBC deep anticyclonic eddies.
- Barotropic instability significantly contributes to the growth of the deep anticyclonic eddies.

*Felipe's current affiliations: UTas-CSIRO PhD Program, IMAS, UTas & AAPP, UTas & ARC CLEX, Hobart, Tas, AU.
†Dante's current affiliations: Univ. Brest, CNRS, Ifremer, IRD, Laboratoire d'Océanographie Physique et Spatiale (LOPS), IUEM, F29280, Plouzané, FR.

Corresponding author: Felipe Vilela da Silva, `felipe.vilela.silva@alumni.usp.br`

Abstract

The Deep Western Boundary Current (DWBC) is the main component of the deep limb of the Atlantic Meridional Overturning Circulation (AMOC). Off northeast Brazil, the DWBC breaks up into southwestward-propagating anticyclones. In this study, we investigate the breakup mechanism with hydrographic observations, eddy-resolving numerical model outputs, and theory. Here, we present a quasi-synoptic map of geostrophic velocities and stream function at the DWBC core level between 2.5°S and 11°S. We observe, in horizontal distributions of velocities, that the DWBC breakup site is linked to a topographic feature of the Brazilian continental margin centered at 8°S: the Pernambuco Plateau. Moreover, both observations and model outputs hint at a possible DWBC separation near the Pernambuco Plateau preceding anticyclone genesis. We test, with three different theories from the literature, whether or not the DWBC separates at 8°S. The results of the tests converge to indicate that the DWBC undergoes a local and intermittent inertial separation while contouring the Pernambuco Plateau. Downstream of its separation at the plateau, the DWBC sheds eddies similarly to previously reported laboratory experiments. In addition, a regional analysis of energy transfer shows that barotropic instability significantly contributes to the anticyclones growth between 8°S and 13°S. Analysis of the energy budget and separation of waters related to the AMOC pathways into the basin interior provide a better understanding for later studies about heat fluxes and ventilation in the deep tropical South Atlantic.

Plain Language Summary

The Deep Western Boundary Current transports southward the cold and dense waters linked to the deep limb of the Atlantic Meridional Overturning Circulation. Among many properties, these waters transport energy from the Northern to the Southern Hemisphere, thousands of meters below the surface. Along the deep ocean off northeast Brazil, this current breaks up into large whirlpools of water that rotate counterclockwise while propagating southwestward. These whirlpools in the ocean are know as eddies. We observe that the eddy formation is linked to a feature of the Brazilian continental margin: the Pernambuco Plateau. Moreover, both shipboard data and numerical model outputs hint at a possible separation of the deep current near the Pernambuco Plateau prior to the eddy formation. We test the separation with theories and the results converge to indicate that the deep current undergoes a local separation off the continental slope while contouring the Pernambuco Plateau. In addition, we present that the eddies grow by feeding off the energy from the deep current. The local separation and regional energy exchange along this deep current contribute to further discussions about the pathways of the Atlantic Meridional Overturning Circulation and heat fluxes in the South Atlantic.

1 Introduction

The Deep Western Boundary Current (DWBC) is the major current transporting the lower limb of the Atlantic Meridional Overturning Circulation (Rintoul, 1991; Gordon, 1991). The DWBC transports the North Atlantic Deep Water (NADW) across the whole Atlantic basin, feeding the Antarctic Circumpolar Current (Tomczak & Godfrey, 1994; Talley et al., 2011). In the northern subtropical Atlantic, the DWBC interacts with the ocean interior by exchanging water properties in a large-scale deep anticyclonic gyre (Biló & Johns, 2019). In addition, the DWBC exports NADW to the Atlantic interior in regions of leakiness as observed south of the Newfoundland Basin (~42°N; Bower et al., 2009) and at the Vitória-Trindade Ridge (~20°S; Garzoli et al., 2015).

Near the Equator, Garzoli et al. (2015) estimated a NADW volume transport of ~14 Sv (1 Sv = 10^6 m^3 s^{-1}). At 5°S, the DWBC flows as a continuous jet, with maximum mean velocities of 0.20 m s^{-1} spanning from 1200 to 4000 m depths (Schott et al., 2005). Further south, Dengler et al. (2004) identified anticyclones at ~2000 m with ~100 km radii using LADCP data and a mooring array at 11°S. Supported by an eddy-resolving numerical model, Dengler et al. (2004) reported that the DWBC breaks up into deep southward-propagating anticyclones at 8°S. Upon reaching the Vitória-Trindade Ridge (~20°S), a portion of the DWBC deflects eastward (Garzoli et al., 2015), carrying NADW into the South Atlantic interior (van Sebille et al., 2012). The main portion of the flow crosses the ridge and continues flowing southward along the South American continental margin as it reorganizes itself as a boundary current (Garzoli et al., 2015).

Although the *in situ* velocity structure of the DWBC has been described upstream (~5°S) and downstream (~11°S) of the breakup site (*e.g.*, Dengler et al., 2004; Schott et al., 2005; Hummels et al., 2015; Garzoli et al., 2015), little is known about the observed DWBC structure and the eddy formation dynamics around 8°S. Curiously, the region between 7.5°S and 9.5°S; 33.5°W and 35°W delimits the location of the most prominent topographic feature over the regional continental slope: the Pernambuco Plateau (Kowsmann & Costa, 1976). This feature marks a significant change in the continental slope orientation.

Previous studies have shown that jets flowing past abrupt changes in the continental margin generally lead to flow separation (*e.g.*, Røed, 1980; Stern & Whitehead, 1990; Garzoli et al., 2015; Solodoch et al., 2020). Røed (1980) presented the influence of the curvature of a cape in the separation of a barotropic boundary current. Stern and Whitehead (1990) combined theory and rotating-tank experiments to explore the necessary conditions for flow separation and the potential consequences (*e.g.*, eddy formation). The DWBC separation from the continental slope was addressed by Garzoli et al. (2015) and Solodoch et al. (2020). Using a numerical model, Garzoli et al. (2015) showed that about 22% of the DWBC leaks to the ocean interior when the current negotiates the topography of the Vitória-Trindade Ridge. Solodoch et al. (2020) investigated the DWBC leakiness in the Newfoundland Basin. Analyzing floats and a high-resolution numerical simulation, the authors found that an "inertial separation" is the mechanism responsible for the DWBC leakiness around the Flemish Cap due to modifications of the mean potential vorticity contours by eddies.

In this study, we propose that the Pernambuco Plateau alters the DWBC flow resulting in eddy genesis. We explore this hypothesis with hydrographic observations, eddy-resolving numerical model outputs, and theoretical concepts. First, we revisit historical observations to map the DWBC between 2.5°S and 11°S. Second, we explore the dynamics induced by the morphology of the Pernambuco Plateau using theory and outputs from a global numerical simulation to seek the mechanisms responsible for the anticyclones' formation. Among other results, we show that the changes in the orientation along the Pernambuco Plateau play a crucial role in separating the DWBC from the continental slope, which ultimately leads to the genesis of the anticyclonic eddies. Finally, we analyze the eddy kinetic energy conversions of the anticyclones while they propagate southwestward between 8°S and 15°S.

2 Observations and Numerical Model Outputs

Given the limited amount of measurements in the deep ocean presented in the literature between 5°S and 11°S, to the best of our knowledge, no horizontal distribution at the DWBC core level has been reported to date using observations in the region. Two previous works used the quasi-synoptic data set that we employ here (Krelling et al., 2020a, 2020b) to mainly explore the dynamics of the North Brazil Undercurrent in the upper layer. They did not they did not focus in the DWBC. We also use outputs from an eddy-resolving numerical model to explore: (i) mechanisms of separation of boundary currents from a curved coastline and (ii) kinetic energy conversions involved in eddy growth.

2.1 The *Oceano Nordeste* I Oceanographic Expedition

We revisit a historical hydrographic data set to present a quasi-synoptic picture of the DWBC velocity and water-mass structure. The *Oceano Nordeste* I (henceforth, ONEI) was carried out by the Brazilian Navy onboard *R/V Antares* between 26 Feb and 21 Mar 2002, occupying eight transects (57 stations) off northeast Brazil. We refer to the ONEI data as quasi-synoptic because it represents a snapshot within the appropriate length and time scales related to the DWBC dynamics. Figure 1a shows the distribution of the ONEI hydrographic stations superimposed on local topography. The red box highlights the Pernambuco Plateau, an extension of the continen-

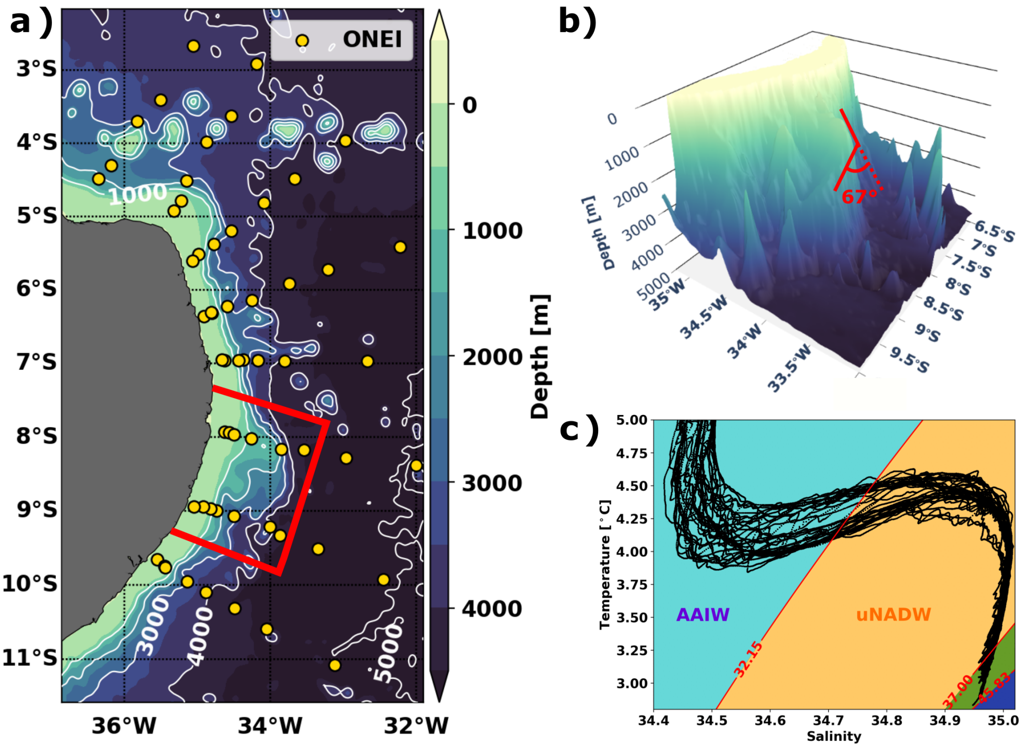

Figure 1. a) Bathymetry map of the study area highlighting the Pernambuco Plateau in the red rectangle, including distribution of the stations and sections of the Brazilian Navy Expedition *Oceano Nordeste* I (yellow filled circles). b) Three-dimensional visualization of the Pernambuco Plateau bathymetry. The red lines illustrate the 67° angle relative to the plateau's orientation (solid line) and the prolongation of the 2000m isobath (dashed line). c) Deep scattered T-S diagram from all the ONEI's stations. The light blue area shows AAIW, the orange area represents uNADW, green highlights mNADW and dark blue distinguishes lNADW. The red lines indicate the interfaces between two adjacent water masses. Bathymetry data obtained from Etopo (Amante & Eakins, 2009).

tal shelf with complex topography that pivots the Brazilian Continental Margin off northeast Brazil (Kowsmann & Costa, 1976). The plateau extends from the continental rise up to 200 m, forming an angle of 67° with the continental slope upstream of 8°S (Fig. 1b).

Hydrographic data were collected with a 24 Hz CTD *SBE 9 Plus* and restricted to the upper 2500 m of the water column. (The ONEI data set is maintained by the Brazilian National Oceanographic Data Center; see data availability statement for details.) Prior to the ONEI expedition, CTD sensors were calibrated at the Instrumentation & Calibration Center of the Oceanographic Institute at the University of São Paulo on 21 Feb 2001.

The distribution of temperature and salinity at intermediate and deep levels obtained during the ONEI (Fig. 1c) virtually covers the whole oceanic region off northeast Brazil. In Figure 1c, the $\sigma_1 = 32.15\,\mathrm{kg\,m^{-3}}$ marks the boundary between the Antarctic Intermediate Water (AAIW) and the NADW (Rhein et al., 1995; Schott et al., 2002). According to Rhein et al. (1995), the NADW is characterized by a local maximum in salinity. Still following the former authors' classification, the ONEI observations (Fig. 1c) capture the upper NADW (between $\sigma_1 = 32.15\,\mathrm{kg\,m^{-3}}$ and $\sigma_2 = 37.00\,\mathrm{kg\,m^{-3}}$) and the middle NADW (between $\sigma_2 = 37.00\,\mathrm{kg\,m^{-3}}$ and $\sigma_4 = 45.83\,\mathrm{kg\,m^{-3}}$). ONEI stations do not capture the lower NADW, although it is present in the region, sandwiched between $\sigma_4 = 45.83\,\mathrm{kg\,m^{-3}}$ and the Antarctic Bottom Water (Schott et al., 2005).

2.2 Assimilative Global Numerical Model Outputs

We used the HYbrid Coordinate Ocean Model (HYCOM; Fox et al., 2002; Cummings, 2005; Cummings & Smedstad, 2013) experiment 19.1 (hereafter, HY19.1), with horizontal resolution $\Delta x = {}^1/_{12}{}^\circ \simeq 10\,\mathrm{km}$ and 40 vertical levels. HY19.1 is forced by the CFSR-NCEP hourly wind and ocean-atmosphere fluxes. It assimilates *in situ* observations (*e.g.*, satellite, ARGO, XBT, moored-buoy data) with the Navy Coupled Ocean Data Assimilation method (Cummings, 2005). We worked with daily outputs from Jan 1997 to Dec 2006, a 10-year period which encompasses the period of the ONEI expedition. To compare the model outputs with previous works in the region (Dengler et al., 2004; Schott et al., 2005; van Sebille et al., 2012; Hummels et al., 2015), we rotated the zonal and meridional velocities in cross-bathymetry sections.

Figure 2 displays vertical sections of 10-year-averaged HY19.1 velocity in cross-bathymetry sections at 5°S and 11°S, and a time series of transport at 11°S. By and large, the model outputs provide a good representation of the main western boundary currents in the domain, namely the North Brazil Undercurrent (NBUC; Silveira et al., 1994; Stramma et al., 1995) and the DWBC. At 5°S (Fig. 2a), the modeled NBUC occupies the upper 1300 m, flowing southward at $0.70\,\mathrm{m\,s^{-1}}$. Underneath, the DWBC spans about 2500 m of water column, flowing in the opposite direction at $0.20\,\mathrm{m\,s^{-1}}$ in its core. This mean configuration is compatible with observations by Schott et al. (2005). South of the Pernambuco Plateau, at 11°S (Fig. 2b), the NBUC core is weaker; the averaged DWBC shows a counter flow related to recurrently-formed anticyclones in the region (Dengler et al., 2004; Schott et al., 2005).

In addition to the 10-year velocity average transects at 5°S and 11°S, we estimated the transport of the modeled DWBC at 11°S (Fig. 2c) imposing the same limits as those proposed by Schott et al. (2005) (for details, see their Figure 8 and surrounding discussion). Our computation yields a 10-year transport of -21.7 ± 16.9 Sv. (Negative values indicate southward transport.) The HY19.1 DWBC compares reasonably to the 27-year transport of -21.3 ± 14.3 Sv calculated by van Sebille et al. (2012) using the OFES (Ocean general circulation model For the Earth Simulator) model, and is in the same range as observations reported by Schott et al. (2005) (-19.1 ± 14.0 Sv from 2000 to 2004) and Hummels et al. (2015) (-19.2 ± 5.2 Sv from 2013 to 2014).

The eddy statistics below rely on the identification and tracking of the model pinched-off anticyclones after reattaching to the slope south of 9.5°S. We developed a simple eddy-tracking algorithm which targets the center of the eddy through a local minimum stream function in a region occupied by rotating features. At 2000 m, between 9.5°S and 10.9°S, 35°W and 32.3°W, we counted 45 eddies during the 10 years of the HY19.1 time series (from 1997 to 2006), with 4.5 ± 0.5

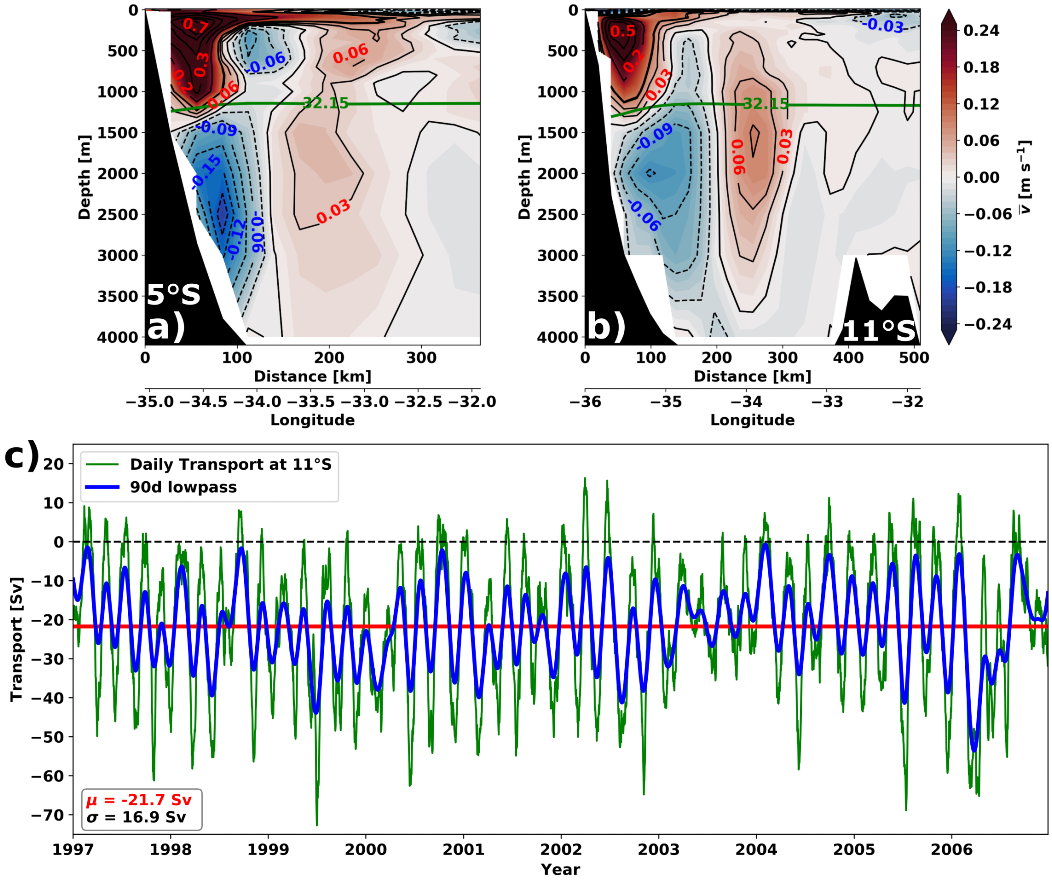

Figure 2. Cross-bathymetry sections of 10-year-averaged rotated velocity from HY19.1 at a) 5°S and b) 11°S. The green line represents the interface between AAIW and NADW. c) DWBC transport time series at a cross-bathymetry section starting at 10.3°S; 35.9°W from HY19.1. The green (blue) line shows the daily (90-day low pass) transport time series from 01/1997 to 12/2006. The μ symbol represents the mean transport (red line), and σ is the standard deviation. The black dashed line highlights the null transport.

eddies released per year. The algorithm detected 1615 snapshots of the eddies propagating within the control area along the 3652 days of the model time series. We detected no apparent seasonal modulation of the eddy-shedding phenomenon.

We computed the mean translation velocity by estimating the distance and time elapsed by the propagating eddies within the control area. We followed a total of 45 eddies in the HY19.1 time series. Throughout 10 years, the anticyclones translate southwestward with a mean velocity of ~0.04 m s^{-1}. This velocity approximately matches the observed translation velocity reported for a 2-year mooring record in Dengler et al. (2004).

To explore the temporal variability in the DWBC transport (see Fig. 2c), we detected the periods of energy peaks in the Morlet power spectrum by performing a wavelet analysis (Torrence & Compo, 1998; Liu et al., 2007) on the DWBC transport time series at 11°S (see Fig. S1). The largest transport variability is 71 ± 3 days, which is consistent with the DWBC anticyclone formation recurrence in the region detected by our eddy-tracking analysis and previously observed by Dengler et al. (2004).

3 The DWBC around the Pernambuco Plateau

To map the DWBC circulation, we applied the classic dynamical method (Pond & Pickard, 2013) to the ONEI data to calculate the geostrophic stream function,

$$\psi = \frac{\Delta\Phi}{f_0}\,, \tag{1}$$

where $\Delta\Phi \stackrel{\text{def}}{=} -\int_{p_0}^{p} \delta dp$ is the geopotential anomaly (δ is the specific volume anomaly, and p_0 is the pressure level of no motion) and f_0 is the average Coriolis parameter.

We interpolated the hydrographic data (temperature and salinity) onto a regular grid using the Fast Marching Method–Objective Analysis (FMM-OA; *cf.* Agarwal & Lermusiaux, 2011) and calculated the potential density. The FMM technique finds the shortest sea distance between two not linearly separated coordinates and improves the standard scalar objective analysis schemes in regions of complex landforms, irregular bathymetry and islands. As in Agarwal and Lermusiaux (2011), we use the distances obtained from the FMM to build the covariance matrix in the distance-dependent analytical correlation function within the OA.

With the 3D density structure, we computed ψ by setting the AAIW-NADW interface σ_1 = 32.15 kg m^{-3} as the isobaric level of no motion and obtained the geostrophic velocities,

$$(u, v) \stackrel{\text{def}}{=} (-\psi_y, \psi_x)\,, \tag{2}$$

where subscripts indicate the partial derivatives in the Cartesian (x, y) directions. We selected the 32.15 kg m^{-3} isopycnal as the level of no motion since it marks the depth of a meridional reversal flow near the continental slope (*cf.*, Section 2.a.1 in Schott et al., 2005). In addition, we enforced free-slip boundary conditions at the 1900m isobath through the objective analysis mapping (Carter & Robinson, 1987), with correlation length = 167 km (*cf.* Eq. 13 in Silveira et al., 2000). The free-slip boundary condition enforces that the continuity of the flow is conserved (*i.e.*, $\vec{u}\cdot\nabla\vec{u} = 0$) and it preserves the DWBC structure observed by the field of purely geostrophic velocities (shown in Fig. S2).

The ONEI geostrophic stream function snapshot in Figure 3a depicts the DWBC reorganizing at 6°S after crossing the Fernando de Noronha Ridge (~4°S), with velocities around 0.10 m s^{-1}. Between 6°S and 8°S, the DWBC narrows down and flows adjacent to the continental slope, with core velocity of ~0.20 m s^{-1}, before sliding over the Pernambuco Plateau. The geostrophic velocity cross-section at 8°S (Fig. 3b) displays the DWBC core with 0.14 m s^{-1} within the upper NADW domain, constrained by the 32.15 kg m^{-3} (σ_1) and the 37.00 kg m^{-3} (σ_2) isopycnals. Further south, Figure 3a shows an 100km-radius and asymmetric anticyclone centered at about 10.5°S in the southernmost transect of the ONEI; this feature occupies mainly the upper NADW, with its core between approximately 1600 and 2000 m (Fig. 3c).

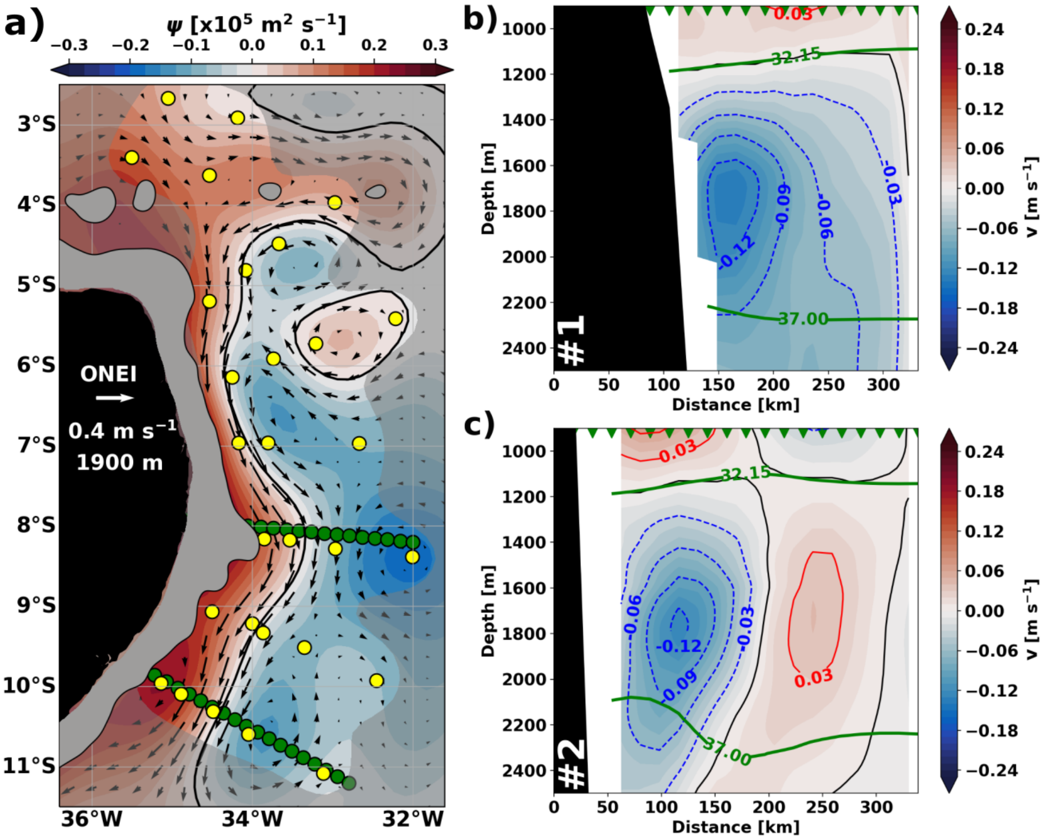

Figure 3. The DWBC observational scenario of anticyclone formation off the Pernambuco Plateau. a) Stream function field ψ [$\times 10^5$ m^2 s^{-1}] at 1900 m obtained through FMM-OA(ONEI). The yellow filled circles indicate the positions of the ONEI stations. The gray shaded area contains the region where the interpolation error is greater than 5%. The dark green circles highlight the locations of transects in b) and c). The velocity fields in b) and c) are the results of geostrophic computation from the 3D-FMM-OA T-S (see text for details). The green lines represent the isopycnals. The dark green triangles illustrate the grid distance. The #1 and #2 symbols represent the 8°S and southernmost transects, respectively.

The results above show similar DWBC settings compared with previous observational studies in the domain (Dengler et al., 2004; Schott et al., 2005; Krelling et al., 2020a). At 5°S, Schott et al. (2005) analyzed a repetition of 9 vertical sections with high horizontal resolution (∼20 km). The authors captured a ∼120km-wide mean DWBC with a velocity of 0.20 m s^{-1} at the core level. At 11°S, the DWBC eddy asymmetry was first reported by Dengler et al. (2004), and detailed by Schott et al. (2005), who presented a mean section with the coastal lobe more than twice as fast as the oceanic lobe. Krelling et al. (2020a) used ONEI observations to describe cross-stream velocities at 6°S and 9°S. To bypass sampling resolution issues, the authors objectively interpolated shipboard-ADCP measurements with geostrophic estimates and showed a DWBC with maximum velocity of 0.20 m s^{-1}. To avoid contamination of our geostrophic estimates by ageostrophic and other higher-frequency motions, we decided to present only the geostrophic component of the flow. Our vertical sections (Fig. 3b,c) depict a DWBC upstream and downstream of the Pernambuco Plateau (at 8°S and 10°S, respectively) with morphometric characteristics similar to those from aforementioned studies. However, the DWBC maximum velocities in ONEI are at least a factor of 1/3 smaller. This underestimation is possibly due to the coarse spatial resolution between the ONEI hydrographic stations (∼50 km).

Despite being derived from geostrophic stream function estimates, the novelty revealed by the ONEI data set is the first quasi-synoptic horizontal scenario of the deep circulation off northeast Brazil. Figure 3a reproduces different aspects previously observed (*e.g.*, Dengler et al., 2004; Schott et al., 2005; Krelling et al., 2020a), and highlights a new one: a possible separation of the DWBC off the Pernambuco Plateau. This snapshot tracks the DWBC axis (represented by ψ = 0 in Fig. 3a) where, at 7°S, the current flows 44 km offshore of the continental slope. Immediately north of the center of the plateau (8°S), the DWBC axis sits 61 km distant from the slope (Fig. 3a). This setting suggests a possible separation mechanism acting on the DWBC at 8°S, with consequences for the flow downstream.

We acknowledge that one snapshot is not enough to fully attest to the existence of such a mechanism. Therefore, we now turn to a numerical model time series to investigate: (i) whether or not the DWBC separates and leaks oceanward at 8°S and (ii) which mechanisms drive the anticyclone genesis.

4 The Modeled DWBC off northeast Brazil

4.1 The DWBC Crossing of the Pernambuco Plateau

Encompassing the ONEI period, we computed the stream function ψ (2) through a Helmholtz velocity decomposition algorithm based on Li et al. (2006). Here, we also calculated the relative vorticity $\zeta \overset{\text{def}}{=} \nabla^2\psi$ to further diagnose the events following the DWBC crossing of the Pernambuco Plateau. Figure 4 displays a sequence of snapshots at 2000 m from the model stream function and relative vorticity normalized by $|f|$. The HY19.1 snapshots between 20 Jan 2002 and 20 Feb 2002 (Fig. 4) reproduce similar patterns captured by the ONEI observation (Fig. 3a).

On 20 Jan 2002 (Fig. 4a), the DWBC flows adjacent to the continental slope, bordering the Pernambuco Plateau at about 0.20 m s^{-1}. Downstream of the plateau, an anticyclone marked by positive $\frac{\zeta}{|f|}$ occupies the region offshore at 10°S (Fig. 4e). The overall magnitude of the Rossby number ($R_o = \frac{\zeta}{|f|}$) in Figure 4e-h shows that the geostrophic balance holds in the region. The DWBC anticyclone in formation at 8°S with $R_o \sim 0.33$ (Fig. 4e) recalls the value reported for the North Brazil Current eddies at 5°N ($R_o = 0.36$; Silveira et al., 2000). This value is larger than the ones usually found in subtropical midlatitudes. However, it clearly shows that the anticyclones are still driven by geostrophy, in more likely gradient balance within the eddies.

Ten days later (Fig. 4b,f), the scenario is the most similar to the ONEI (Fig. 3a): south of 8°S, the main axis of the DWBC moves away from the slope, with its inner portion reattaching at 9.5°S (see the negative vorticity of the inner lobe in Fig. 4f). Further south, the anticyclone traveled ∼50 km southward.

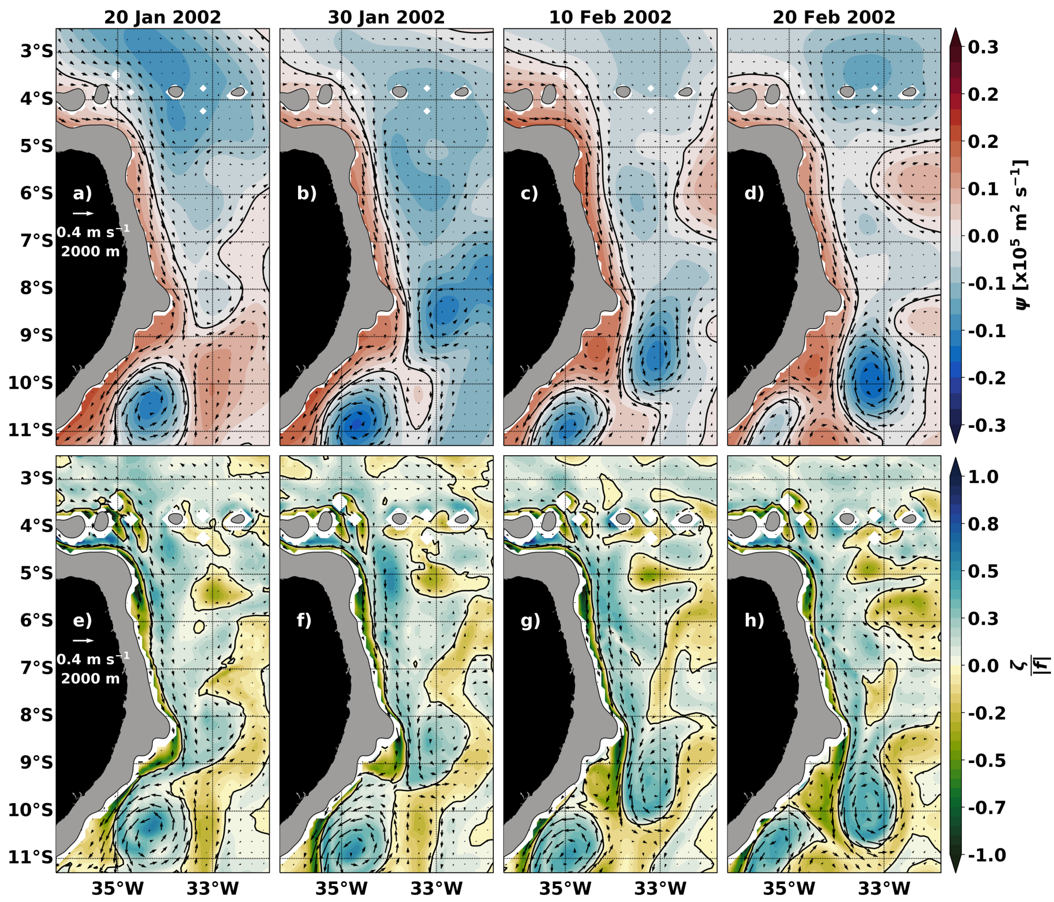

Figure 4. The anticyclone genesis from HY19.1 at 2000 m. Upper row (a,b,c,d panels): stream function fields ψ [$\times 10^5$ m^2 s^{-1}]. Lower row (e,f,g,h panels): rossby number $\left(\frac{\zeta}{|f|}\right)$. The solid contour designates the null ψ and ζ. The date of each realization is on top of the panel.

On 10 Feb 2002, the DWBC backflips into another anticyclone, with closed contours forming downstream of the Pernambuco Plateau (Fig. 4c). Squeezed by the old and the newly formed anticyclone, negative $\frac{\zeta}{|f|}$ points to a small cyclone on the shadow of the plateau (Fig. 4g; see this and other events in the animation in the Movie S1). Figure 4d depicts the anticyclone shed on 20 Feb 2002, briefly interrupting the DWBC flow at the lee of the Pernambuco Plateau, as indicated by the diverging arrows at 10°S (Fig. 4d,h). The old anticyclone continued traveling southward and left the region by the end of February. Note that part of the DWBC seems to separate from the continental slope as it crosses the plateau in Figure 4 and every eddy formation periods (see Movie S1), suggesting a link between the separation process and the formation of the anticyclones.

4.2 The Mean DWBC Pathway

To assess the mean DWBC pathway, we computed the 10-year mean stream function ψ and potential vorticity (PV) from the simulation near the Pernambuco Plateau. Since PV is a dynamical tracer that is conserved in the absence of dissipation or forcing, its distribution can hint at the dynamical processes modifying the flow along its path. Here, we use Ertel's PV definition for large and mesoscale flows (Pedlosky, 1987),

$$q = (\zeta + f)\, b_z, \tag{3}$$

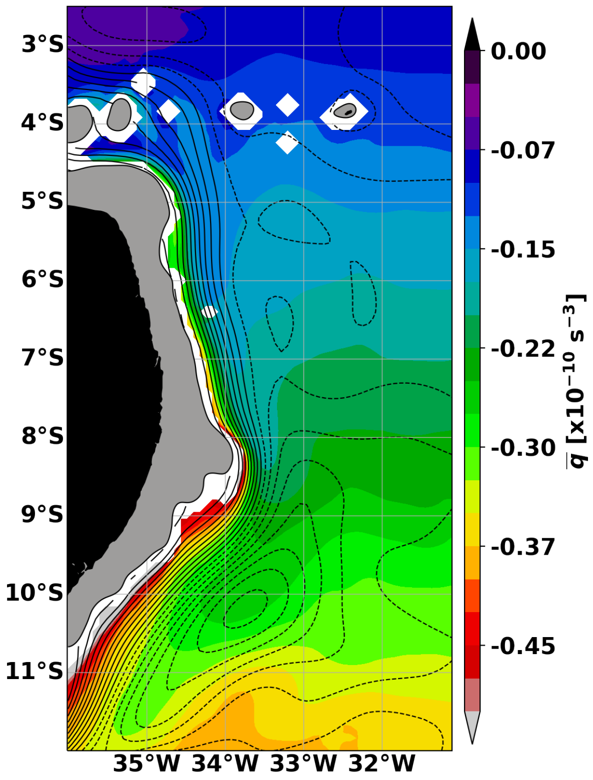

Figure 5. The HY19.1 dynamical fields at 2000 m. The 10-year mean potential vorticity $\overline{q}$ [$\times 10^{-10}$ s^{-3}] and stream function (solid/dashed lines indicate positive/negative values).

where b_z is the vertical buoyancy gradient ($b \overset{\text{def}}{=} -g\rho/\rho_0$ is the buoyancy). Figure 5 presents the potential vorticity distribution at the DWBC velocity core at 2000 m.

Upstream of the Pernambuco Plateau, the streamlines and PV contours are mostly parallel along the continental slope (Fig. 5), which hints at the steadiness of the circulation upstream of the plateau. As the DWBC flows southward, the mean DWBC crosses a region with strong gradient in the mean PV field (Fig. 5). South of 8°S, a feature telltale of separation events appears, the modeled DWBC streamlines spread offshore as the current overshoots the plateau similarly to the ONEI observations (Fig. 3a).

In addition, the crossing of the plateau is marked by a significant decrease in the mean PV content along the mean DWBC streamlines (Fig. 5) because the PV contours veer offshore forming a prominent low-PV tongue in the area (*i.e.*, larger horizontal gradients of q). The intersection of q and ψ lines ($\nabla\overline{q} \times \nabla\overline{\psi} \neq 0$) could indicate that the flow is not on a steady state or that the flow is under a constant forcing (*cf.* Rhines & Holland, 1979; Napolitano et al., 2019). The eddy-forcing is likely to be reducing the flow's PV content and forcing the mean flow southward at the region where the DWBC sheds the anticyclones near the plateau.

Overall, Figure 5 depicts the deformation of PV contours as the DWBC core contours the Pernambuco Plateau, particularly from a PV tongue that spreads between 7°S and 9°S. According to Pickart and Huang (1995), the distortion of the PV field near capes hints at inertial separation of the mean streamlines. Next, we evaluate the conditions for a separation of the DWBC streamlines at the Pernambuco Plateau.

5 The DWBC Separation

Previous studies addressed the separation of boundary currents on a curved coastline (*e.g.*, Røed, 1980; Stern & Whitehead, 1990; Solodoch et al., 2020). Røed (1980) derived a condition for boundary current separation due to curvature effects. Ten years later, Stern and Whitehead (1990) combined theory and laboratory experiments to explore the upstream conditions that might lead to flow separation, including its post-separation effects, such as eddy formation. Recently, Solodoch et al. (2020) analyzed the cross-bathymetry velocity from a numerical model and proposed an empirical scaling analysis to investigate the inertial separation mechanism for the DWBC at the Flemish Cap. In this section, we test these theories to investigate the DWBC separation at 8°S and the anticyclone genesis downstream of the Pernambuco Plateau.

5.1 The DWBC Inertial Separation

Both observations and model outputs suggested a local DWBC separation in Sections 3 and 4. Previous studies explored inertial separation using the semigeostrophic approximation (*e.g.*, Ou & De Ruijter, 1986; Pickart & Huang, 1995). However, semigeostrophy does not hold in regions where cross-stream variations are larger than (or equivalent to) along-stream changes. Recently, Solodoch et al. (2020) expanded the Pickart and Huang's (1995) theoretical arguments to evaluate the DWBC separation and leakiness around the Flemish Cap. The novel evaluation is based on analysis of the PV field, coupled behavior between the cross-bathymetry velocity and the control exerted by bathymetry, and a scaling analysis (Solodoch et al., 2020).

Proceeding to investigate conditions leading to inertial separation, we now explore the theoretical arguments discussed above for the DWBC at the Pernambuco Plateau. Figure 6 evaluates the role played by the Pernambuco Plateau in driving the DWBC offshore upstream of the topographic bump. As for the distortion of the PV field as an argument for inertial separation (Pickart & Huang, 1995), Figure 6a depicts the deformation of the 10-year mean PV contours related to the DWBC core, especially around the Pernambuco Plateau. Following Solodoch et al.'s (2020) extension of Pickart and Huang's (1995) theory, Figure 6b shows the cross-bathymetry velocity (v_{CROSS}) at the westernmost continuous PV contour ($-0.35\times10^{-10}\,\text{s}^{-3}$) south of 6.5°S. We employ this contour as a proxy for the shape of the 2000m isobath along the DWBC axis. From 6.5°S to nearly 8°S, the DWBC flows almost parallel to the isobaths (as indicated by the low v_{CROSS} in Fig. 6b). At 8°S, v_{CROSS} increases sharply in the offshore direction at the plateau's north face towards its corner. Downstream of the plateau's elbow (at ≈ 8.3°S), v_{CROSS} drops to zero. South of 9.5°S, v_{CROSS} is negative (Fig. 6a). This pattern is consistent with the inshore propagation and reattachment of the downstream anticyclones, which does not invalidate the quest for the DWBC separation at 8°S. Reattachment cannot be excluded even if part of the flow separates: "weak" reattachment is expected for a "large-angle" bump (Solodoch et al., 2020) which does not fit the DWBC setting along the Pernambuco Plateau.

In Figure 6b, we relate v_{CROSS} with the changes in orientation of the 2000m isobath in the downstream r direction, *i.e.*, $\partial\Theta/\partial r$, where Θ is the angle along the smoothed 2000m isobath in the downstream r direction (represented by the orange contour in Fig. 6a). The highest v_{CROSS} values span along the upstream sector of the plateau, with a maximum of $\sim$0.06 m s^{-1} immediately north of the corner, represented by the maximum $\partial\Theta/\partial r \approx 2°\,\text{km}^{-1}$ (Fig. 6b). To estimate the influence of the plateau's curvature on v_{CROSS}, we computed the lead-lag correlation between the cross-bathymetry velocity and the variation of the slope orientation. Figure 6c depicts the strongest correlation of 0.87 at -28 km, meaning that changes in the isobath angle are sensed by the DWBC v_{CROSS} about 30 km upstream of the Pernambuco Plateau edge, pushing the DWBC offshore from there on.

The evaluation of the two theoretical criteria performed here is similar to the one in Solodoch et al. (2020), who addressed the DWBC inertial separation in the Flemish Cap by evaluating the correlation between the cross-bathymetry velocity and the curvature and steepness gradient of the slope. As in Solodoch et al. (2020), our results are consistent with separation driven by an angled plateau, indicated by strong (lagged) correlations between the v_{CROSS} velocity toward off-

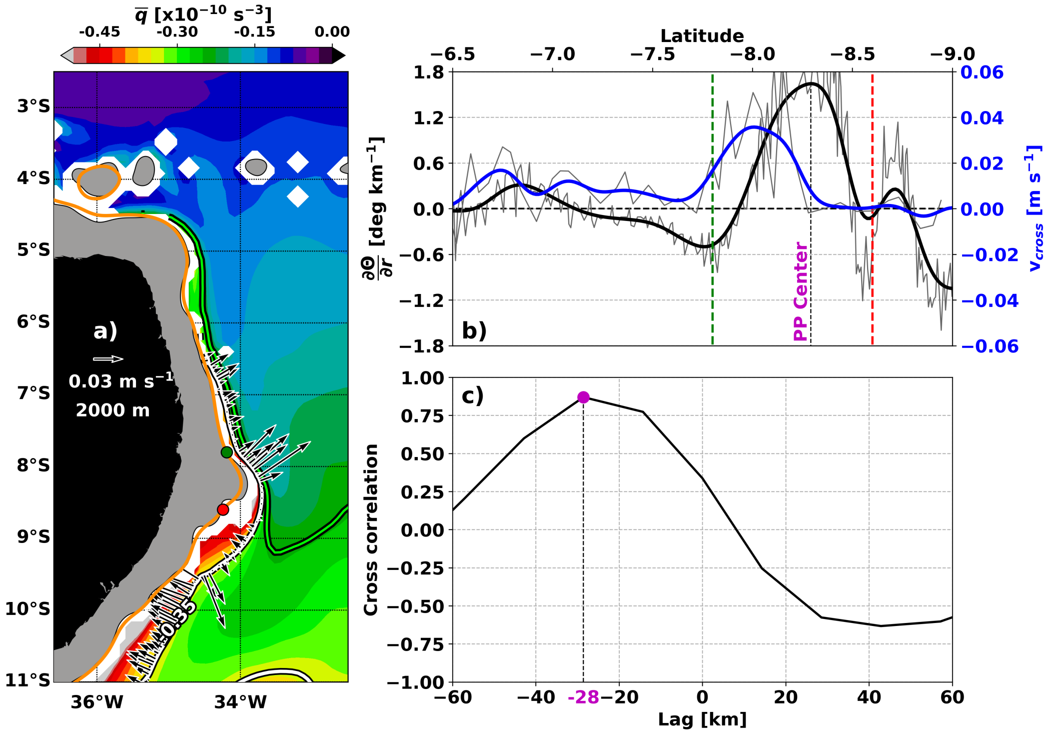

Figure 6. a) The 10-year mean potential vorticity $\overline{q}$ [$\times 10^{-10}$ s^{-3}]. The white line highlights the westernmost continuous potential vorticity contour (-0.35 $\times$ 10^{-10} s^{-3}) between 6.5°S and 11°S at 2000 m. The green contour within the black line marks the spreading of the PV tongue. The arrows indicate the 10-year mean velocity component (v_{CROSS}) normal to the selected PV contour. The orange contour represents a smoothed bathymetry along 2000 m. b) Meridional profiles of the v_{CROSS} and the changes in orientation along the smoothed 2000m isobath $\partial\Theta/\partial r$ [deg km^{-1}]. Green and red dashed lines correspond to the circles in panel (a), which demark the Pernambuco Plateau (PP) limits. c) The lead-lag cross correlation between $\partial\Theta/\partial r$ and v_{CROSS}. Purple circle marks the distance of the maximum correlation to the PP center.

shore and sharp changes in the 2000m isobath orientation (Fig. 6c). However, these correlations could be an indication of DWBC meandering preceding anticyclone formation (see Fig. 4) instead of a proper separation process.

In addition to the limitation detailed above, for the case of a jet around a cape, semigeostrophy is not valid if the radius of curvature (R_c) is smaller in magnitude than the width W of the jet (Solodoch et al., 2020). The Pernambuco Plateau-DWBC setup (*i.e.*, $R_c = -30$ km, and $W =$ 100 km) falls within this limitation. (The DWBC turns clockwise at the Pernambuco Plateau, hence R_c is negative.) Therefore, the diagnostic of inertial separation based solely on applying semigeostrophic arguments in the scenario of Figure 6 is either compromised or valid only in certain portions of the domain. To circumvent the limitations of semigeostrophy, Solodoch et al. (2020) proposed to evaluate the inertial separation via a scaling analysis. In this case, a separating streamline must be present.

To evaluate a separating streamline, we refer back to Figure 4 where part of the DWBC separates during periods of anticyclones formation. In contrast, in the 10-year mean q and ψ scenarios (Fig. 5), the streamlines do not completely separate from the continental slope. Instead, they spread offshore and smoothly contour the Pernambuco Plateau. Separating streamlines tend to be smeared and averaged out in the mean scenario due to the anticyclones' southwestward propagation and intermittency of eddy genesis south of the Pernambuco Plateau. Thus, we propose to assess the PV along separating streamlines during the DWBC eddy genesis events. We track these events by seeking local minima of ψ within closed contours (*i.e.*, anticyclonic features) between 6.5°S and 8.5°S in the eddy-tracking algorithm discussed in Section 2.2. The algorithm returned 289 snapshots in the area of eddy genesis related to each of the 45 eddies formed through the 10 years of the model time series.

The outputs related to eddy genesis were then averaged over time to evaluate q and ψ (Fig. 7a). In this scenario, a portion of the DWBC separates from the continental slope south of 8°S to form an anticyclonic circulation (Fig. 7a). Moreover, the separating streamlines approximately follow the veered PV contours eastward once they leave the western boundary (follow the white 0.27×10^4 m^2 s^{-1} contour between 6°S and 9°S in Figure 7a for reference).

To evaluate this possible inertial separation, we estimated the mean PV budget at 2000 m during the eddy genesis. For inertial processes, the budget can be simplified as the balance between the mean PV advection and convergence of eddy-PV fluxes (*e.g.*, Solodoch et al., 2020),

$$\overline{\mathbf{u}} \cdot \nabla \overline{q} = -\nabla \cdot (\overline{\tilde{\mathbf{u}}\tilde{q}}) \tag{4}$$

where $\mathbf{u}$ is the horizontal velocity vector, the overbar represents the time-average of the eddy genesis snapshots, and tildes are the perturbations around the time-mean. Equation (4) is known as the Turbulent Sverdrup Balance (Rhines & Holland, 1979).

Similarly to model representations of the DWBC in the South and North Atlantic (van Sebille et al., 2012; Solodoch et al., 2020; Biló et al., 2021), the HY19.1 simulation shows that the Turbulent Sverdrup Balance is valid at the DWBC core from 5°S to 11°S (Fig. 7b,c), and indicates that the separation is indeed an inertial process. Following the $\psi = 0.27\times10^4$ m^2 s^{-1} streamline reaching the plateau (Fig. 7a), we note a strong decrease in the PV content that allows the DWBC to detach from the western boundary in a counterclockwise direction along the anticyclonic eddies. As the anticyclones grow and propagate (see Fig. 4 or Movie S1), they probably generate the PV and velocity perturbations necessary for changing the mean flow. Downstream the separation of the boundary, both terms in Eq. (4) decrease up to two orders of magnitude (Fig. 7b,c). These patterns indicate that the flow mainly follows the PV contours before flowing over a well PV-homogenized area (*i.e.*, Eq. (4) ≈ 0).

Since part of the DWBC flow seems to separate the continental slope inertially during eddy genesis (Fig. 7), we can further evaluate the separation following the scaling analysis given by Solodoch et al. (2020). The authors show that inertial separation takes place when reductions oc-

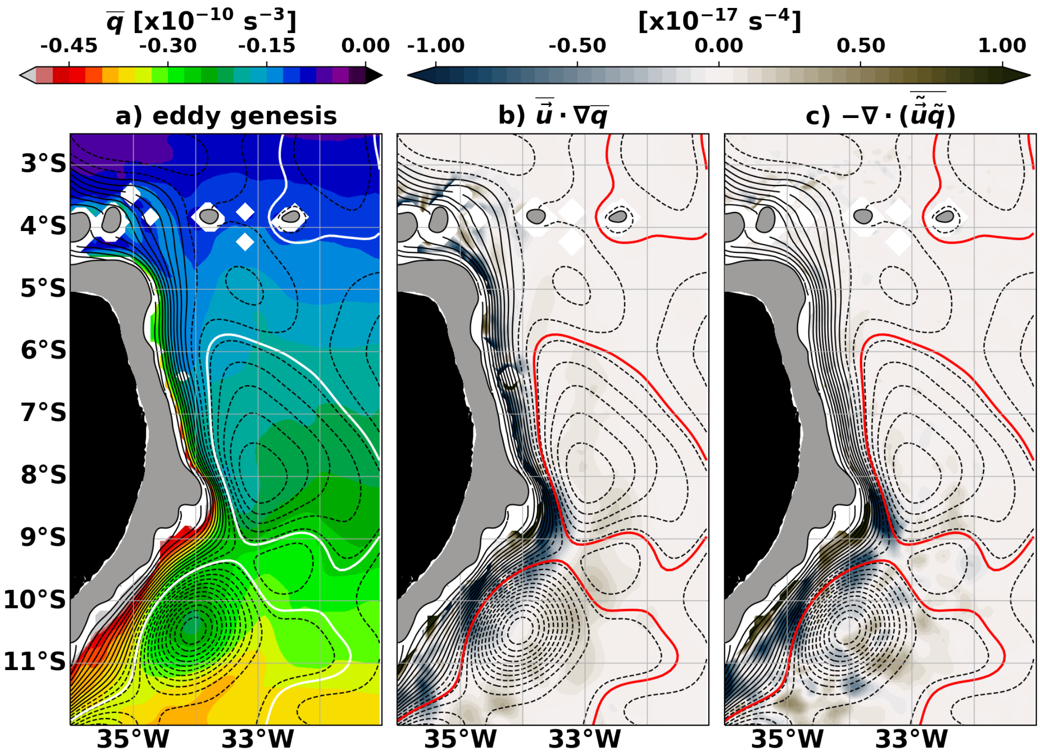

Figure 7. The HY19.1 composites of eddy genesis at 2000 m. a) Potential vorticity $\overline{q}$ [$\times 10^{-10}$ s^{-3}]. b) Mean PV advection $\overline{\mathbf{u}} \cdot \nabla\overline{q}$ [$\times 10^{-17}$ s^{-4}]. c) Divergence of eddy PV fluxes $\nabla \cdot (\overline{\tilde{\mathbf{u}}\tilde{q}})$ [$\times 10^{-17}$ s^{-4}]. The black contours represent the mean streamlines: solid (dashed) lines indicate positive (negative) values. The white and red contours highlight the 0.27×10^4 m^2 s^{-1} mean streamline.

cur in

$$\Delta U \approx U\frac{W}{R_c} - fW\frac{dh}{h}, \tag{5}$$

where ΔU is the downstream change in cross-current shear integrated in the positive n direction, and n is oriented normally to the streamlines. The scaling analysis indicates that inertial separation is expected if $|\Delta U|$ is relatively larger than $|U|$ (Solodoch et al., 2020). Another indication of the separation is that the current width is greater than the curvature radius magnitude ($W > |R_c|$). We select the quantities displayed in Eq. (5) from the eddy genesis composite: the $U = 0.15\,\mathrm{m\,s^{-1}}$ is the velocity scale for the DWBC, $W = 100\,\mathrm{km}$ is the current's width upstream of the Pernambuco Plateau, and $R_c = -30\,\mathrm{km}$ is the streamline radius of curvature. (The clockwise turn of the DWBC at the Pernambuco Plateau results in negative R_c.) We estimate the DWBC thickness ($h = 3\,\mathrm{km}$) and the isopycnal steepening across the current ($dh = 351.5\,\mathrm{m}$) within the vertical limits by the $\sigma_1 = 32.15\,\mathrm{kg\,m^{-3}}$ isopycnal at its top and $\sigma_1 = 32.54\,\mathrm{kg\,m^{-3}}$ at its bottom in a vertical section near the center of the Pernambuco Plateau (8°S).

Applying the DWBC values above to Eq. (5) yields $U\frac{W}{R_c} = -0.50\,\mathrm{m\,s^{-1}}$ and $-fW\frac{dh}{h} = 0.24\,\mathrm{m\,s^{-1}}$. As a result, $\Delta U = -0.26\,\mathrm{m\,s^{-1}}$. In this case, ΔU is $0.11\,\mathrm{m\,s^{-1}}$ higher in magnitude than U. In addition, $W = 3.33|R_c|$. Therefore, both criteria strongly suggest that the DWBC along the Pernambuco Plateau undergoes an inertial separation during the eddy genesis scenario.

While the curvature term in Eq. (5) adds to a drop in ΔU, due to the clockwise curvature of the current, the vertical stretching term acts in the opposite direction. The dynamical balance between these two terms offers a possible explanation for the partial separation of the streamlines, where only the outer lobe (positive ζ) of the DWBC separates and originates the anticyclones.

We now compare our results with the original study by Solodoch et al. (2020). In their study at the Flemish Cap, both the curvature and vertical stretching terms reduce the velocity per unit distance offshore (ΔU). While the Solodoch et al. (2020) results represent an uninterrupted series where the DWBC separates and leaks offshore permanently, the values reported herein correspond to an average of intermittent events, where the DWBC separates prior to the eddy genesis. Here, the application of the Solodoch et al. (2020) scaling analysis indicates that the DWBC separates inertially while crossing the Pernambuco Plateau during the eddy genesis events and anticyclone shedding.

5.2 The Curvature Effect of the Pernambuco Plateau

Røed (1980) explored how the curvature of a cape influences the separation of a homogeneous, inviscid and rotating fluid (*e.g.*, a barotropic boundary current) from an irregular wall. To assess the separation process, Pratt and Whitehead (2007) adapted Røed's geometric parameter as

$$\hat{R} = \tanh\left(\frac{2R_d}{W_c}\right), \tag{6}$$

where R_d is the jet's deformation radius and W_c is the wall's curvature radius. The Pernambuco Plateau W_c approximates to 30 km for the 2000m-isobath bend between 8°S and 8.5°S. Contrary to the curvature radius of the jet (R_c), the wall's curvature (W_c) is positive at capes (Røed, 1980). For R_d, we use the value of a theoretical jet. The flow dynamics can be approximated by the relative vorticity—or barotropic-like dynamics—in the presence of a small stretching term. Imposing this setting for the DWBC regime, we can think of the local dynamics as an upside-down equivalent-barotropic flow with a rigid lid dividing two separate regimes: the NBUC and the DWBC, which would preserve the baroclinic length scales. Under these considerations, we applied the classical Flierl (1978) calibration of layered models to obtain an equivalent-barotropic deformation radius of 210 km. In particular, we applied the calibration due to bottom topography forcing (*cf.* Sec. 4 in Flierl, 1978).

According to Røed (1980) and Pratt and Whitehead (2007), the flow separates when $\hat{R} > 0.999$. Under such conditions (*i.e.*, $W_c << R_d$) in Eq. (6), the flow is not able to follow the sup-

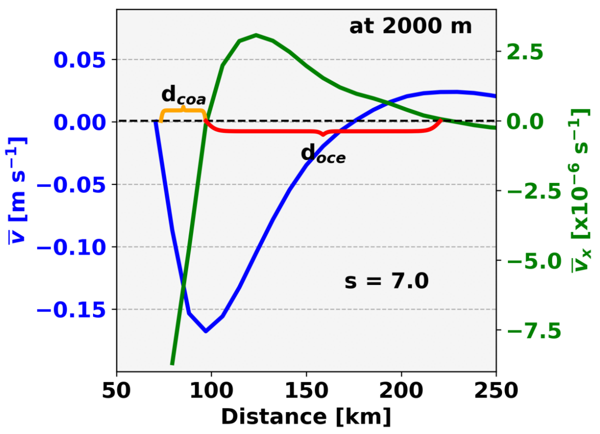

Figure 8. The 10-year mean of velocity $\overline{v}$ [m s^{-1}] (blue) and vorticity $\overline{v}_x$ [$\times 10^{-6}$ s^{-1}] (in green) profiles at 2000 m and 7°S. The d_{COA} and d_{OCN} indicate the width of the coastal and oceanic $\overline{v}_x$ lobes, respectively. The horizontal axis represents the distance from the coast.

porting wall and separation occurs. Røed (1980) suggested the application of this theory to deep currents along slopes, which fits the DWBC crossing of the Pernambuco Plateau.

Inserting our study parameters into Eq. (6) yields $\hat{R} > 0.999$, thus indicating that a DWBC-like equivalent-barotropic jet separates from the continental margin at 8°S. Downstream of the separation point, Røed's theory breaks down and cannot be used to explain what happens after the separation. To start filling this gap, the theory proposed by Stern and Whitehead (1990) addresses the downstream consequences of a separating jet.

From rotating tank experiments and a theoretical model, Stern and Whitehead (1990) revealed that a barotropic jet flowing along a vertical wall sheds eddies as it crosses a corner with an obtuse angle. The authors proposed two parameters to evaluate whether or not the jet separates from the adjacent wall: the angle θ and the ratio s. The angle θ is the angle between the projections of the wall in the upstream and downstream sectors. We estimated the θ angle between the projection of the Pernambuco Plateau and its downstream wall, with $\theta = 67°$ (see the schematics and plateau description in Fig. 1b). The critical vorticity ratio

$$s = \frac{d_{\mathrm{OCE}}}{d_{\mathrm{COA}}} \tag{7}$$

is the ratio between the width of the offshore and inshore vorticity lobes immediately upstream of the corner (Stern & Whitehead, 1990). The d_{OCE} and d_{COA} represent the width of the oceanic and coastal vorticity lobes, respectively. We compute s using the relative vorticity width in an idealized jet. The theoretical jet here is similar to the one we explored in Røed's theory (*i.e.*, a DWBC-like equivalent-barotropic jet) following the setting of small stretching term.

To approximate the DWBC conditions upstream the Pernambuco Plateau to the idealized jet, we used the HY19.1 10-year mean velocity, bounded by $\sigma_1 = 32.15$ kg m^{-3} on the top and 4000 m on the bottom, in a transect at 7°S. The mean cross section presents the velocity core of -0.15 m s^{-1} at 2000 m (Fig. 8 and Fig. S3). The horizontal profile at the core (Fig. 8) depicts the two vorticity lobes, computed as the zonal derivative of the cross-transect velocity v_x for the oceanic and coastal lobes, d_{OCE} = 123.5 km and d_{COA} = 17.6 km, which yields $s = 7.0$.

Stern and Whitehead (1990) built a θ–s regime diagram to evaluate possible separation of the flow under the proposed criteria. (The authors used the angle $\alpha = \theta/180 + 1$.) According to the authors, the regions in which the flow separates or not are delimited by a relation between θ and s, namely the critical angle $\theta_c = |45°| \pm 5°$ and the critical vorticity ratio $s = 0.33$. Even for small θ, a flow with $s > 1$ always present separation at a corner. As presented above, the plateau wall angle is $\theta_c = 67°$ and, from Eq. (7), $s = d_{\text{OCE}}/d_{\text{COA}} = 7.0$. Those values strongly advocate for the separation of the DWBC-like jet at the Pernambuco Plateau.

Stern and Whitehead (1990) also showed that a barotropic rotating jet facing a sharp corner will shed eddies. The configuration for the separating cases in Stern and Whitehead's (1990) experiments shows the flow shedding anticyclones, cyclones and/or dipoles. This scenario is consistent with the anticyclone formation at the DWBC breakup site depicted in the HY19.1 snapshots (Fig. 4). In the scenario presented in those images, the apparent separation of the main DWBC axis downstream of the Pernambuco Plateau precedes the anticyclone's shedding. Additionally, not only are anticyclones formed, but dipoles are also generated as consequence of the roll-up of the cyclonic (coastal) and anticyclonic (oceanic) DWBC lobes. With $s = 7.0$, we conclude that the anticyclones are far larger than the cyclones because the coastal vorticity lobe is narrower than the oceanic one (compare Fig. 4g with Fig. 1c in Stern & Whitehead, 1990). After the full shedding of the eddies, the cyclones vanish as the anticyclones reattach to the continental slope and propagate southwestward. In contrast, for the non-separating cases, Stern and Whitehead (1990) showed the shedding of one initial cyclone, with additional cyclones being formed along the wall. There is no resemblance between the non-separating scenario and the DWBC case analyzed here.

5.3 The Separation Verdict and Possible Consequences

By combining the results from the tests of the DWBC separation at 8°S in three distinct theories (Solodoch et al., 2020; Røed, 1980; Stern & Whitehead, 1990), we find that the DWBC undergoes a local, intermittent inertial separation while contouring the Pernambuco Plateau. The separation of the DWBC waters might result in leakiness of a fraction of the current to the ocean interior as it occurs at the Flemish Cap (Bower et al., 2009; Solodoch et al., 2020) and the Vitória-Trindade Ridge (van Sebille et al., 2012; Garzoli et al., 2015). At the Pernambuco Plateau, the flow quasi-periodically separates and then sheds anticyclonic eddies, which travel southwestward during a DWBC non-separation period.

During eddy formation and propagation, the ψ contours cross PV contours in the eye of the anticyclone (Fig. 7a). The advection of PV contours may suggest unstable conditions associated with the formation and propagation of these features. In addition, we note a change in sign of $\partial q/\partial n$, which may also point to barotropic instability playing a key role in the eddy dynamics (*e.g.*, Vallis, 2017). This pattern is consistent with those of Biló and Johns (2020), who reported an inversion in the mean zonal PV gradient, possibly related to instability processes driving the formation of eddies and meanders that propagate southward along the DWBC at 26.5°N. Next, we focus on the DWBC anticyclones and the processes triggered by the DWBC separation, which lead to eddy formation, propagation, and growth.

6 On the Life Span of the DWBC Anticyclones

6.1 The Eddy Corridor from the Pernambuco Plateau to 15°S

The ONEI observations adjacent to the Pernambuco Plateau (Sec. 3) confirmed that 8°S is the latitude of the DWBC breakup into anticyclones, as first shown by Dengler et al. (2004) from numerical model outputs. Downstream of the plateau, the propagation of these anticyclones can be identified by velocity anomalies. We computed the HY19.1 eddy zonal velocity ($\tilde{u}$) as the anomaly from a slowly-varying "mean" velocity obtained through the application of a 60-day low-pass filter.

Following the shape of the 2000m isobath, we built a path between 5°S and 15°S along the Brazilian continental margin. To build the path, we use the time-mean stream function contour $\psi = 0$ as a proxy for the mean position of the DWBC. Then, we projected this path to the east and to the west to set the boundaries of the eddy corridor. The shift for these east and west projections rely on the previous reported radii of the anticyclone (∼100 km; Dengler et al., 2004). The

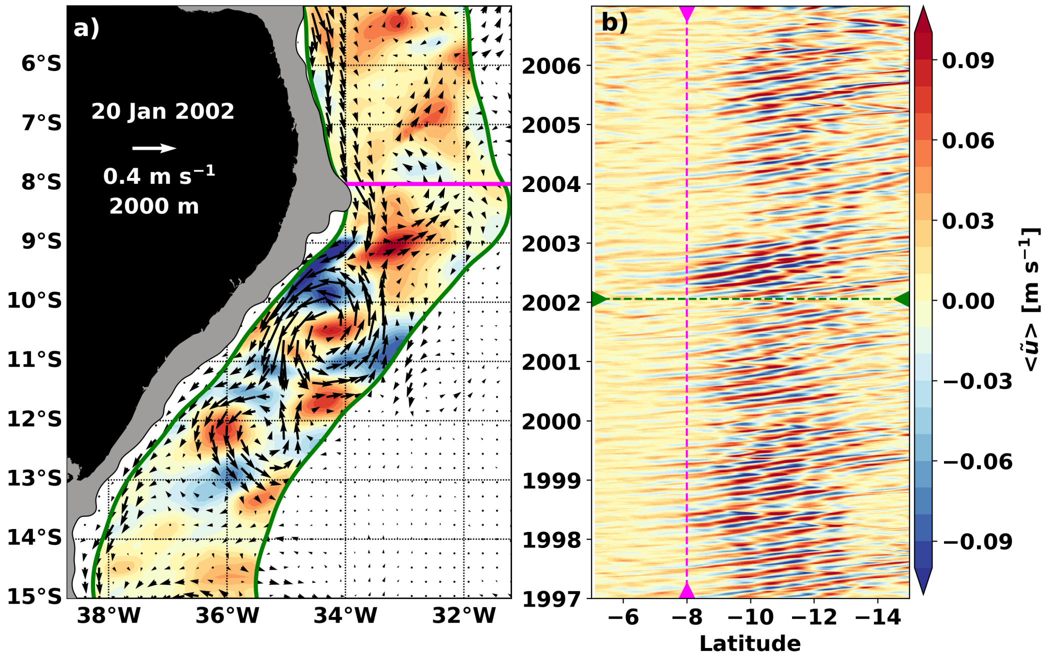

Figure 9. The propagating DWBC anticyclones at 2000 m. a) Snapshot on 20 Jan 2002 with total velocities in vectors superimposed on a map of zonal velocity perturbations $\tilde{u}$ [m s^{-1}] along the corridor delimited by the green lines bordering the band occupied by the meandering DWBC and its anticyclones. b) Hovmöller diagram from 1997 to 2007 showing longitudinal mean of eddy velocity $<\tilde{u}>$ inside the green pathway between 5°S and 15°S. Green dashed line indicates the day presented in (a). Magenta line (map and Hovmöller) highlights the latitude where the anticyclones are shed (8°S).

45 anticyclones depicted by the eddy tracking algorithm are within these limits. In this “eddy corridor” downstream of 8°S, the anticyclones propagate southwestward until either disappearing south of 13°S or reaching 15°S, as shown in Figure 9.

In Figure 9a, we chose a simulation snapshot that captures an eddy in formation at 8°S and two eddies previously shed and centered at 10.5°S and 12.5°S. Along the DWBC path snapshot (Fig. 9a), we represent the total velocity by the arrows and the zonal eddy component by the colormap. The total velocity vectors display the DWBC parallel to the continental slope between 5°S and 7.5°S and recirculating into an eddy centered at 8°S. We depict positive $\tilde{u}$ patches in the south and negative $\tilde{u}$ values north of this recirculation, indicating an anticyclonic feature. The anticyclonic pattern repeats itself throughout the eddy corridor in another two pinched-off anticyclones between 9°S and ~13°S. South of 13°S, the eddy velocities decrease and the DWBC reappears, closely following the continental slope.

A Hovmöller diagram displaying 10 years of $\tilde{u}$ along the designated path shows that eddy genesis and propagation occur throughout the time series (Fig. 9b). We tracked perturbations upstream of the Pernambuco Plateau and note weaker alternating $\tilde{u}$ patterns north of 8°S. These weak signals propagate along with the DWBC, drastically increasing downstream of the DWBC separation point. This behavior further indicates that the Pernambuco Plateau is responsible for the DWBC anticyclone genesis and growth. Therefore, we interpret these weaker velocity bands upstream as remote perturbations related to the DWBC crossing the Fernando de Noronha seamount chain at 4°S. These might trigger the separation and eddy shedding at 8°S (see Fig. 4 and Movie S1). Most of these perturbations dissipate around 13°S, but some continue propagating downstream (Fig. 9b). Further application of other eddy tracking algorithms that compute radii, amplitudes, and shapes of the eddies (Mason et al., 2014; Trott et al., 2018; de Marez et al., 2019) would potentially give insight on the merge, splitting, and dissipation of the anticyclones.

As these weak perturbations flow past the Pernambuco Plateau along with the DWBC, they begin to increase to a maximum of $\tilde{u}$ between 9°S and 10°S. All along the eddy corridor, these perturbations maintain their strength, with small variations along the path. The weak perturbations may amplify due to instability processes (Philander, 1990). In the DWBC, barotropic instabilities have been shown to play a role in regional dynamics (Solodoch et al., 2020; Biló et al., 2021; Schulzki et al., 2021). Solodoch et al. (2020) calculated the energy conversion associated with the DWBC leaking and anticyclone formation around the Flemish Cap. At this location, the eddies' growth results from barotropic conversion through Reynolds stress work. South of the Flemish Cap, between 26.5°N and 16°N, Schulzki et al. (2021) used an eddy-rich ocean model and revealed that barotropic instabilities dominate over baroclinic instabilities within the DWBC, with a gain in eddy kinetic energy resulting from strong horizontal shear. Moreover, the presence of the DWBC rubbing against the Pernambuco Plateau further advocates for the importance of horizontal shear instabilities, as they can draw energy from western boundary currents into eddies (*e.g.*, Mata et al., 2006; Napolitano et al., 2019).

6.2 The Growth Mechanism for the DWBC Anticyclones

Generally related to instability processes, eddies can be a product of energy conversions (*e.g.*, Phillips & Rintoul, 2000; Mata et al., 2006; Silveira et al., 2008; Chen et al., 2014; Napolitano et al., 2019). South of Australia, in the Antarctic Circumpolar Current, Phillips and Rintoul (2000) analyzed 2 years of mooring data and found baroclinic conversion as the main mechanism for the growth of eddies. Along the East Australian Current, from model outputs and altimetry data, Mata et al. (2006) suggested that both barotropic and baroclinic instabilities drive the growth of eddies as they propagate southward. From moored current meters, Silveira et al. (2008) found that baroclinic instability is primarily responsible for a Brazil Current meander growth between 22°S and 25°S. In a detailed assessment of the energetics in the Gulf Stream and Kuroshio extensions, Chen et al. (2014) showed that both barotropic and baroclinic conversions act on the mean flow, driving kinetic energy production. Using a regional numerical simulation off east Brazil, Napolitano et al. (2019) showed that eddies grew from perturbations fed by the mean flow of the Intermediate Western Boundary Current, mainly through lateral shear.

Motivated by the discussion closing the previous section, we aim to investigate the role played by barotropic instabilities in the DWBC eddies' life cycle. We evaluate conversions within the kinetic energy budget by analyzing barotropic conversions as a mechanism for the DWBC anticyclones growth. We follow Vallis (2017) and Napolitano et al. (2019) to calculate the horizontal shear production,

$$HSP = -\rho_1 \left[\overline{(\tilde{v}^2 - \tilde{u}^2)} \psi_{xy} + \overline{\tilde{v}\tilde{u}} (\psi_{xx} - \psi_{yy}) \right], \tag{8}$$

where $\rho_1 = 1032.43\,\mathrm{kg\,m^{-3}}$ is the potential density referenced at 1000 m for the DWBC core. We recall that ψ is the model stream function and the tilde denotes the eddy component from a slowly-varying 60-day mean. We acknowledge that HSP alone does not close the regional eddy kinetic energy budget ($^{DE_{KE}}/_{Dt} \approx 0$) of the system. However, based on the weak stratification of the deep ocean, we take HSP as the major player in the eddy-genesis process. In addition, we estimated the HY19.1 eddy vertical velocities at 2000 m and found small values; consequently, we can assume that the integrated vertical terms are negligible compared with the horizontal terms. To test our assumption, we also calculated the horizontal buoyancy production (Fig. S4), which is on average 10 times smaller than HSP. The model outputs indicate that the barotropic instabilities rule over the baroclinic in the region of eddy formation (S6), and thus we will not address its role in the present energy balance.

To evaluate the role of HSP in the growth process, we opt to split the eddy corridor from Figure 9 into two major dynamical paths: coastal (the inner portion in Fig. 10a) and oceanic (outer portion in Fig. 10a). This follows from our investigations of the inertial DWBC separation in Section 5, where we found that only the offshore portion of the DWBC rolls up into eddies, whereas

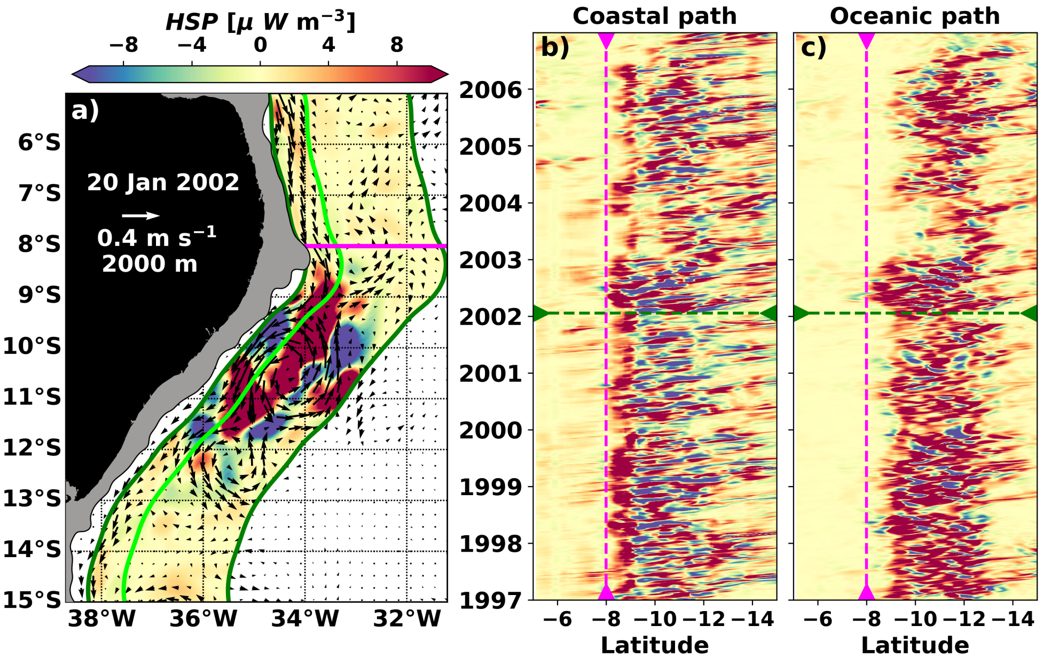

Figure 10. The horizontal shear production HSP [μ W m^{-3}] map and time series at 2000 m. Positive values represent mean-to-eddy kinetic energy conversions. The magenta lines highlight the 8°S latitude. a) Snapshot on 20 Jan 2002. Dark green contours demark the eddy corridor limits. b,c) The HSP Hovmöllers west and east of the light green line in the map represent the coastal and oceanic paths, respectively. The daily time series result from computing longitudinal HSP means in each path. The dark green line in the Hovmöllers indicates the day reproduced by the map.

the inner portion continues along the continental slope. To separate these two paths, we use the $\psi \approx 0$ contour (see Fig. 4). By considering the split approach, we compare the horizontal energy conversions due to HSP occurring at each DWBC lobe during anticyclone formation and propagation along the continental slope.

In Figure 10a, we present the HSP map at 2000 m on 20 Jan 2002, the same date already presented in Figure 9a. This snapshot exemplifies our understanding of the eddy formation, shedding and propagation with the addition of the barotropic conversion values. The HSP pattern in this snapshot shows that energy conversion within the DWBC is far more intense downstream of 8°S (Fig. 10a). In other words, the energy conversions occur at the southern face of the Pernambuco Plateau, where the DWBC partial separation triggers the genesis of the anticyclones. At 8.5°S; 33.5°W, $HSP > 0$ (Fig. 10a) points to eddy growth by drawing kinetic energy from the mean DWBC.

Downstream of the plateau, a fully developed anticyclone spins between 9°S and 11.5°S (Fig. 10a). Throughout the center of this eddy, mean kinetic energy (M_{KE}) is converted to eddy kinetic energy (E_{KE}). The $HSP > 0$ patches dominate the oceanic path (Fig. 10a). In contrast, on the coastal path (which is also the coastal lobe of this eddy), $HSP < 0$ is responsible for the E_{KE} conversion back to the M_{KE}. This seems to drive an intensification of the "non-separated" coastal branch of the mean DWBC (Fig. 10a). We speculate here as to whether or not this process is linked to eddy-topography interactions.

Between 11.5°S and 13°S, an older, smaller anticyclone presents similar $HSP < 0$ on the coastal path. Weaker eddy-to-mean conversions appear also on the oceanic path, which we postulate could be related to eddy decay, since eddies virtually vanish south of 13°S in the Hovmöller series along both paths (Fig. 10b,c).

Next, we appeal to the entire 10-year time series to assess the conversion processes. The coastal and oceanic Hovmöllers of HSP along the isolated paths (Fig. 10b,c) show a noisy pattern between 9°S and 13°S, with alternating bands of mean-to-eddy and eddy-to-mean conversions throughout the time series. This noisy pattern occurs mainly during eddy propagation and interaction with the continental slope as illustrated in the horizontal HSP snapshot (Fig. 10a). Nevertheless, coherent patterns appear in each path, related to specific events during the life span of the anticyclones.

From 1997 to 2007, multiple $HSP > 0$ events along the coastal path indicate perturbations drawing energy from the mean flow as the DWBC separates at 8°S, immediately downstream of the Pernambuco Plateau (Fig. 10b; *e.g.*, Napolitano et al., 2019). The M_{KE} to E_{KE} conversions attest to the growth of the DWBC anticyclones. In the coastal path (Fig. 10b), an $HSP > 0$ band extends from 8°S to about 9°S, where the anticyclones drain energy from the mean DWBC as it crosses the Pernambuco Plateau.

The findings above resemble the results reported by Magalhães et al. (2017) for the Brazil Current. Using 10 years of HY19.1 outputs, the authors evaluated the eddy-mean flow interaction from both barotropic and baroclinic instabilities in the upper ocean off southeast Brazil. They found M_{KE} to E_{KE} conversions associated with flow interactions with prominent bathymetric features. Downstream of the DWBC eddy-genesis site, the eddies move southwestward and reattach to the slope. We note that they present an inversion in the energy conversion regime, depicted by southward-propagating bands of $HSP < 0$ (Fig. 10b). This is again similar to the Brazil Current behavior reported by Magalhães et al. (2017), which showed energy conversions of opposite sign (*i.e.*, acceleration of the time-mean flow) up- and downstream of these features. This eddy-topography interaction may push the anticyclones southwestward (Fig. 10b).

In contrast to the coastward (and northern) eddy lobe, the oceanward (and southern) eddy lobe appears to redraw kinetic energy from the DWBC between 10°S and 11°S. This process maintains the eddy structure (Fig. 10b; see also Fig. 10a). South of 13°S, the coastal lobe alternates the sign of kinetic energy conversion throughout the time series (Fig. 10b). Kinetic energy conversions are notably weaker south of this latitude and more irregular in time (Fig. 10b).

On the oceanic path Hovmöller, an area with no significant conversions occupies the time series from 5°S to 9°S (Fig. 10c). The pinched-off eddies enter the eastern margin corridor south of 9°S and continue to grow, feeding off the mean flow along the eddy axis. During propagation, the eddies convert M_{KE} to E_{KE} between 9°S and 13°S throughout the 10 years of simulation (Fig. 10c). HSP nearly vanishes downstream of 13°S, with isolated eddies surviving and eventually reaching 15°S (Fig. 10c; see also Fig. 9b). Mean-to-eddy conversions also dominate HSP in the upper layers of the Brazil Current, extending south from 15°S to 38°S, as evaluated by Oliveira et al. (2009) from 13 years of drifter observations.

The simple analysis performed here did not pinpoint the mechanisms of decay and death of the anticyclones. However, the sparse E_{KE} to M_{KE} conversions at 10°S and 12°S on both coastal and oceanic paths indicate regions of eddy weakening (Fig. 10b,c). These conversions toward the mean kinetic budget are similar to the reports for notorious eddy decay regions, such as the Kuroshio and the Gulf Stream extensions (*e.g.*, Chen et al., 2014; Kang & Curchitser, 2015, respectively).

6.3 The DWBC Anticyclones' Net HSP

Due to the DWBC barotropicity reported in the North Atlantic (Schulzki et al., 2021) and the analyses shown above, we consider HSP as the main mechanism at play during the DWBC anticyclones growth and propagation. The patchy patterns displayed by the HSP Hovmöllers (Fig. 10b,c) indicate an intricate interplay between mean-to-eddy and eddy-to-mean conversions, with

M_{KE} to E_{KE} conversion dominating the oceanic path, and E_{KE} to M_{KE} on the coastal path. It is noteworthy, however, that due to the significantly wider oceanic area within the eddy-corridor, the DWBC anticyclones tend to grow mainly via HSP (*i.e.*, $HSP > 0$).

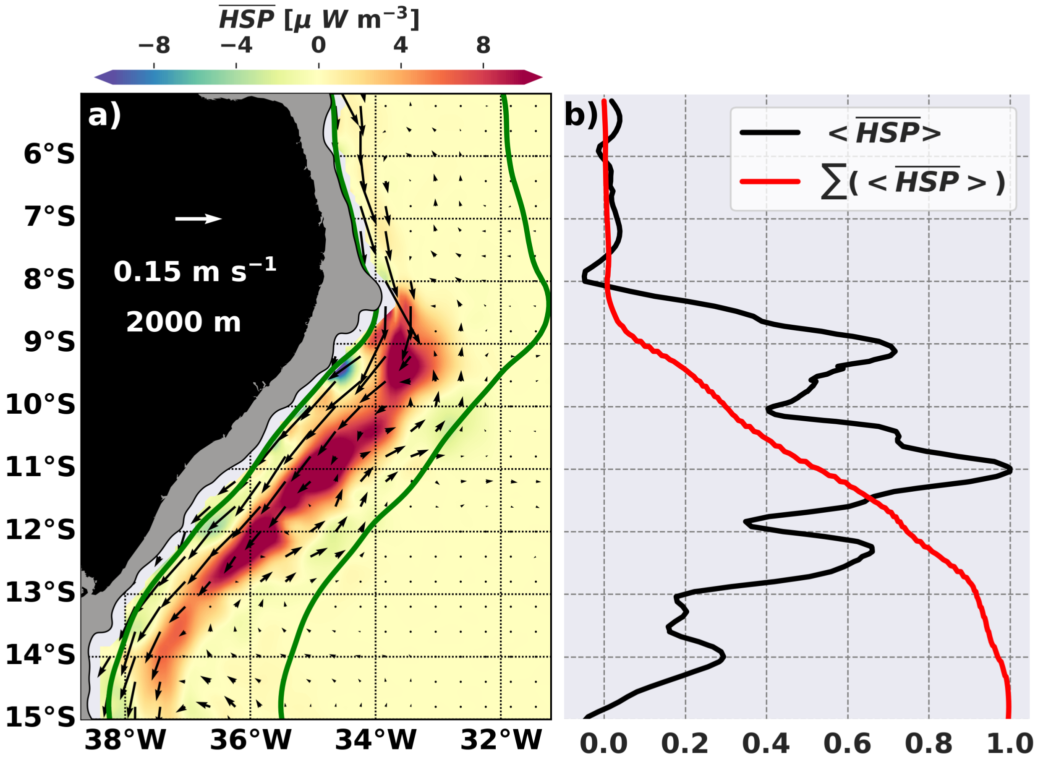

Figure 11. The net horizontal shear production $\overline{HSP}$ [μ W m^{-3}] at 2000 m. Positive values represent M_{KE} to E_{KE} conversions. a) The distribution of a 10-year HSP mean. The dark green contours demark the eddy corridor limits. The vectors reproduce the 10-year mean of velocities. b) The black line represents the longitudinal mean (<>) of $\overline{HSP}$ within the eddy corridor limits, and the red line shows the cumulative sum of the black line values $\Sigma(<\overline{HSP}>)$.

The 10-year mean $\overline{HSP}$ in Figure 11 illustrates the net shear production of the nearly barotropic DWBC dynamics along both paths. First, the horizontal distribution in Figure 11a links the DWBC separation in the Pernambuco Plateau to the anticyclones' initial growth at 8°S. (Note the strong velocity pointing offshore at the corner of the plateau.) Second, south of the eddy formation site, $\overline{HSP} < 0$ highlights a pool of E_{KE} to M_{KE} conversions next to the slope between 9°S and 10°S, where the DWBC eddies try to reinsert into a possible mean flow (Fig. 11a). This attempt to strengthen the mean DWBC occurs throughout nearly all the coastal segments, albeit much more weakly downstream of 10°S (Fig. 11a).

From 8°S to 13°S, remnant northeastward velocities delimit the eastern border of the eddy corridor (Fig. 11a). Within these limits, the time-mean field (Fig. 11a) illustrates that the M_{KE} to E_{KE} conversions are constrained to the centers of the eddies, leaving a trail of positive net HSP (Fig. 11a). Diagnostics of the longitudinally averaged $\overline{HSP}$, normalized by their maximum, throughout the eddy corridor display a roller-coaster pattern in Figure 11b (the <> denotes the spatial averaging). North of 8°S, $<\overline{HSP}>$ is nearly constant (Fig. 11b). Between the Pernambuco Plateau and 13°S, $<\overline{HSP}>$ is inarguably positive, with three distinct peaks (Fig. 11b), which are followed by a decrease at 13°S (Fig. 11). The local maxima in these three peaks contribute to the gradual increase of the cumulative $<\overline{HSP}>$ (Fig. 11b). The local minima at 10°S and 12°S (Fig.

11b) register a contribution from $HSP < 0$, which coincides with regions where the coastal path displays strong E_{KE} to M_{KE} (Fig. 11a and Fig. 10b).

The cumulative $< \overline{HSP} >$ flat line upstream of 8°S confirms that anticyclone growth initially occurs downstream of the plateau (Fig. 11b). Entering the eddy corridor, the cumulative curve increases exponentially from 8°S to 13°S, reaching a maximum near 14°S. South of 14°S, $\Sigma(<\overline{HSP}>)$ stabilizes, meaning that barotropic conversions through HSP are weak or nonexistent from this latitude southward. As we anticipated, the net HSP reinforces the argument that the eddy kinetic energy budget ${}^{DE_{KE}}/_{Dt} \approx 0$ depends on additional terms, such as the contribution from baroclinic conversions (*e.g.*, Lüschow et al., 2019; Schulzki et al., 2021), dissipation due to eddy decay and mixing (*e.g.*, Kang & Curchitser, 2015; Spingys et al., 2021) and advection by the mean flow out of the domain (*e.g.*, Chen et al., 2014; Napolitano et al., 2019).

7 Final Remarks

The *Oceano Nordeste* I (ONEI) oceanographic expedition presented a quasi-synoptic map of geostrophic velocities and stream function at the DWBC core level off northeast Brazil. ONEI cross-bathymetry transects of geostrophic velocity at 8°S and 10°S confirm that the DWBC breakup occurs at 8°S. At this latitude, the Pernambuco Plateau stands as the main obstacle in the DWBC's path. The quasi-synoptic patterns are correctly reproduced by the HYCOM 19.1 outputs, which show the breakup of the DWBC downstream of the plateau leading to eddy genesis. A potential vorticity analysis shows that the DWBC PV structure in the domain deforms downstream of the Pernambuco Plateau with a pronounced PV tongue, which is an indication of flow separation from topography (Pickart & Huang, 1995).

Our analyses of the HYCOM 19.1 outputs also suggest that the DWBC undergoes a local, intermittent separation while contouring the Pernambuco Plateau and it is a crucial process to the formation of deep eddies downstream of the plateau (Movie S1). Along separating DWBC streamlines during eddy-formation periods, a modeled mean PV budget indicates that the Turbulent Sverdrup Balance is valid and this balance shows that part of the DWBC separates inertially off the Pernambuco Plateau. We also evaluated the inertial separation empirically by employing a scaling analysis (Solodoch et al., 2020). The result of the scaling analysis evaluation shows that the downstream changes in the cross-stream horizontal velocity shear further supports the arguments for the DWBC inertial separation at 8°S. In addition, the relation between the deformation radius of a DWBC-like jet and the Pernambuco Plateau curvature radius (Røed, 1980), and the ratio between its coastal and oceanic vorticity lobes widths immediately upstream of the plateau (Stern & Whitehead, 1990) corroborate the separation argument. The latter theoretical relationship also provides evidence of appropriate conditions for the anticyclone genesis downstream of the jet separation off the supporting wall.

Downstream of the separation, the DWBC offshore lobe, with positive relative vorticity, folds into anticyclones which travel southwestward. To verify whether or not barotropic instability is part of the eddy growth, we evaluated the local kinetic energy conversions at the DWBC core depth. South of the separating latitude at 8°S, mean-to-eddy energy conversions through horizontal shear production (HSP > 0) contribute to the growth of the anticyclones. During propagation, changes in HSP sign along the slope highlight bands of E_{KE} to M_{KE} conversions acting to strengthen the coastal lobe downstream of the Pernambuco Plateau. A positive net HSP within the eddy corridor between 8°S and 13°S suggests that barotropic instability is a mechanism relevant to the eddies' dynamics after the anticyclone genesis. This positive net HSP fuels the E_{KE} budget. We encourage further studies to explore the regional energy budget and settle the terms which compensate for the net E_{KE} produced during the DWBC anticyclones' life cycle in the deep tropical South Atlantic, a region intimately related to the Atlantic Meridional Overturning Circulation and climate variability.

Finally, the separation and possible leakiness of the DWBC waters (*i.e.*, NADW) modify the pathways of the Atlantic Meridional Overturning Circulation's lower limb (as in Bower et al., 2009; Garzoli et al., 2015). These pathways are pivotal to understand the basin-scale heat fluxes and deep ocean ventilation. As seen in other regions, the DWBC eddies promote connectivity and water exchanges between the deep western boundary layer and the ocean interior (*e.g.*, Solodoch et al., 2020; Biló et al., 2021). Therefore, it is reasonable to speculate that the eddy formation and growth processes (*e.g.*, the geophysical instability described in this study) might play a relevant role in the deep South Atlantic's heat storage and carbon residence time. As the next step, we suggest future studies to investigate the role of the anticyclonic eddies in the DWBC leakiness and water mass transformation near the Pernambuco Plateau.

8 Open Research

The *in situ* data used in this study are available at the National Oceanographic Data Center (Banco Nacional de Dados Oceanográficos) maintained by the Brazilian Navy. The Brazilian Navy shares the data at `https://www.marinha.mil.br/dhn/?q=en/node/216` with a request to `chm.bndo@marinha.mil.br`. The global numerical model outputs from HY19.1 incorporated in the research are found at `https://www.hycom.org/data/glbu0pt08/expt-19pt1`.

Acknowledgments

The authors are grateful for the scientific contributions from discussions with A. Solodoch, G.R. Flierl, and I.T. Simoes-Sousa, in addition to the IOUSP examination board corrections from B.M. Castro and P.S. Polito. We dedicate this work to the memory of B.M. Castro, who devoted more than 4 decades to the education of several generations of physical oceanographers in Brazil.

The authors acknowledge the sampling efforts by the crew and scientists in the Brazilian Navy *R/V Antares* during the ONEI expedition. FVS acknowledges FAPESP (Process Number: 2018/06153-7) and CAPES (Process Number: 88881.199872/2018-01) for financial support. ICAS acknowledges support from CNPq (Grant 307814/2017-3), Projeto SUBMESO (CNPq 442926/2015-4), Projeto REMARSUL (CAPES 88882.158621/2014-01), and Projeto VT-Dyn (FAPESP 2015/21729-4). DCN acknowledges support from the TRIATLAS project, which has received funding from the European Union's Horizon 2020 research and innovation programme under grant agreement No 817578. PWSN acknowledges the support from CAPES (Process Number: 88887.474629/2020-00) and FAPESP (Process Number: 2020/04315-0). TCB is funded by the National Science Foundation under grant OCE1258823. AG, ICAS and FVS acknowledge the support of SMAST and UMass Dartmouth for hosting FVS during the first semester of 2019, when part of these analyses were initially carried out.

References

Agarwal, A., & Lermusiaux, P. F. J. (2011). Statistical field estimation for complex coastal regions and archipelagos. *Ocean Modelling*, *40*(2), 164–189. (`https://doi.org/10.1016/j.ocemod.2011.08.001`)

Amante, C., & Eakins, B. W. (2009). ETOPO1 1 Arc-Minute Global Relief Model: Procedures, Data Sources and Analysis. NOAA Technical Memorandum NESDIS NGDC-24. *National Geophysical Data Center, NOAA.*, *1*. (`https://doi.org/10.7289/V5C8276M`)

Biló, T. C., & Johns, W. E. (2019). Interior pathways of Labrador Sea water in the North Atlantic from the Argo perspective. *Geophysical Research Letters*, *46*(6), 3340–3348. (`http://doi.org/10.1029/2018GL081439`)

Biló, T. C., & Johns, W. E. (2020). The Deep Western Boundary Current and adjacent interior circulation at 24°–30°N: Mean structure and mesoscale variability. *Journal of Physical Oceanography*, *50*(9), 2735–2758. (`http://doi.org/10.1175/JPO-D-20-0094.1`)

Biló, T. C., Johns, W. E., & Zhao, J. (2021). Dynamics of Deep Recirculation Cells Offshore of the Deep Western Boundary Current in the Subtropical North Atlantic (15–30N).

Journal of Physical Oceanography, *51*(1), 131–145. (http://doi.org/10.1175/JPO-D-20-0184.1)

Bower, A. S., Lozier, M. S., Gary, S. F., & Böning, C. W. (2009). Interior pathways of the North Atlantic meridional overturning circulation. *Nature*, *459*(7244), 243–247. (http://doi.org/10.1038/nature07979)

Carter, E. F., & Robinson, A. R. (1987). Analysis Models for the Estimation of Oceanic Fields. *Journal of Atmospheric and Oceanic Technology*, *4*(1), 49–74.

Chen, R., Flierl, G. R., & Wunsch, C. (2014). A Description of Local and Nonlocal Eddy–Mean Flow Interaction in a Global Eddy-Permitting State Estimate. *Journal of Physical Oceanography*, *44*(9), 2336–2352. (http://doi.org/10.1175/JPO-D-14-0009.1)

Cummings, J. A. (2005). Operational multivariate ocean data assimilation. *Quarterly Journal of the Royal Meteorological Society*, *131*(613), 3583–3604. (https://doi.org/10.1256/qj.05.105)

Cummings, J. A., & Smedstad, O. M. (2013). Variational data assimilation for the global ocean. In *Data assimilation for atmospheric, oceanic and hydrologic applications (vol. ii)* (pp. 303–343). Springer. (https://doi.org/10.1007/978-3-642-35088-7_13)

de Marez, C., L'Hégaret, P., Morvan, M., & Carton, X. (2019). On the 3D structure of eddies in the Arabian Sea. *Deep Sea Research Part I: Oceanographic Research Papers*, *150*, 103057.

Dengler, M., Schott, F., Eden, C., Brandt, P., Fischer, J., & Zantopp, R. J. (2004). Break-up of the Atlantic Deep Western Boundary Current into eddies at 8°S. *Nature*, *432*(7020), 1018–1020. (https://doi.org/10.1038/nature03134)

Flierl, G. R. (1978). Models of Vertical Structure and the Calibration of Two-Layer Models. *Dynamics of Atmospheres and Oceans*, *2*(4), 341–381. (http://doi.org/10.1016/0377-0265(78)90002-7)

Fox, D. N., Teague, W. J., Barron, C. N., Carnes, M. R., & Lee, C. M. (2002). The modular ocean data assimilation system (MODAS). *Journal of Atmospheric and Oceanic Technology*, *19*(2), 240–252. (https://doi.org/10.1175/1520-0426(2002)019<0240:TMODAS>2.0.CO;2)

Garzoli, S. L., Dong, S., Fine, R., Meinen, C. S., Perez, R. C., Schmid, C., . . . Yao, Q. (2015). The fate of the Deep Western Boundary Current in the South Atlantic. *Deep Sea Research Part I: Oceanographic Research Papers*, *103*, 125–136. (https://doi.org/10.1016/j.dsr.2015.05.008)

Gordon, A. L. (1991). The role of thermohaline circulation in global climate change. *In: Lamont–Doherty Geological Observatory 1990 & 1991 Report, Columbia University, Palisades, New York*. (https://doi.org/10.7916/D8M04G8H)

Hummels, R., Brandt, P., Dengler, M., Fischer, J., Araujo, M., Veleda, D., & Durgadoo, J. V. (2015). Interannual to decadal changes in the western boundary circulation in the Atlantic at 11°S. *Geophysical Research Letters*, *42*(18), 7615–7622. (https://doi.org/10.1002/2015GL065254)

Kang, D., & Curchitser, E. N. (2015). Energetics of eddy-mean flow interactions in the Gulf Stream region. *Journal of Physical Oceanography*, *45*(4), 1103–1120. (https://doi.org/10.1175/JPO-D-14-0200.1)

Kowsmann, R. O., & Costa, M. P. d. A. (1976). Estratigrafia sísmica do Platô de Pernambuco. *Revista Brasileira de Geociências*, *6*(2), 95–101. (http://doi.org/10.25249/0375-7536.197695101)

Krelling, A. P. M., Gangopadhyay, A., Silveira, I. C. A., & Vilela-Silva, F. (2020a). Development of a Feature-oriented Regional Modeling System for the North Brazil Undercurrent region (1°-11°S) and its application to a Process Study on the Genesis of the Potiguar Eddy. *Journal of Operational Oceanography.*. (https://doi.org/10.1080/1755876X.2020.1743049)

Krelling, A. P. M., Silveira, I. C. A., Polito, P. S., Gangopadhyay, A., Martins, R. P., Lima, J. A. M., & Marin, F. d. O. (2020b). A Newly Observed Quasi-stationary

Subsurface Anticyclone of the North Brazil Undercurrent at 4°S: The Potiguar Eddy. *Journal of Geophysical Research: Oceans*, *125*(10), e2020JC016268. (https://doi.org/10.1029/2020JC016268)

Li, Z., Chao, Y., & McWilliams, J. C. (2006). Computation of the streamfunction and velocity potential for limited and irregular domains. *Monthly Weather Review*, *134*(11), 3384–3394. (https://doi.org/10.1175/MWR3249.1)

Liu, Y., San Liang, X., & Weisberg, R. H. (2007). Rectification of the bias in the wavelet power spectrum. *Journal of Atmospheric and Oceanic Technology*, *24*(12), 2093–2102. (https://doi.org/10.1175/2007JTECHO511.1)

Lüschow, V., von Storch, J.-S., & Marotzke, J. (2019). Diagnosing the Influence of Mesoscale Eddy Fluxes on the Deep Western Boundary Current in the 1/10°STORM/NCEP Simulation. *Journal of Physical Oceanography*, *49*(3), 751–764. (https://doi.org/10.1175/JPO-D-18-0103.1)

Magalhães, F. C., Azevedo, J. L. L., & Oliveira, L. R. (2017). Energetics of eddy-mean flow interactions in the Brazil Current between 20S and 36S. *Journal of Geophysical Research: Oceans*, *122*(8), 6129–6146. (https://doi.org/10.1002/2016JC012609)

Mason, E., Pascual, A., & McWilliams, J. C. (2014). A new sea surface height–based code for oceanic mesoscale eddy tracking. *Journal of Atmospheric and Oceanic Technology*, *31*(5), 1181–1188.

Mata, M. M., Wijffels, S. E., Church, J. A., & Tomczak, M. (2006). Eddy shedding and energy conversions in the East Australian Current. *Journal of Geophysical Research: Oceans*, *111*(C9). (https://doi.org/10.1029/2006JC003592)

Napolitano, D. C., Silveira, I. C. A., Rocha, C. B., Flierl, G. R., Calil, P. H., & Martins, R. P. (2019). On the Steadiness and Instability of the Intermediate Western Boundary Current between 24 and 18S. *Journal of Physical Oceanography*, *49*(12), 3127–3143. (http://doi.org/10.1175/JPO-D-19-0011.110.1175/JPO-D-19-0011.1)

Oliveira, L. R., Piola, A. R., Mata, M. M., & Soares, I. D. (2009). Brazil Current surface circulation and energetics observed from drifting buoys. *Journal of Geophysical Research: Oceans*, *114*(C10). (https://doi.org/10.1029/2008JC004900)

Ou, H. W., & De Ruijter, W. P. (1986). Separation of an inertial boundary current from a curved coastline. *Journal of Physical Oceanography*, *16*(2), 280–289. (https://doi.org/10.1175/1520-0485(1986)016<0280:SOAIBC>2.0.CO;2)

Pedlosky, J. (1987). *Geophysical Fluid Dynamics* (Vol. 710). Springer. (https://doi.org/10.1007/978-1-4612-4650-3)

Philander, S. G. (1990). El Niño, La Niña, and the Southern Oscillation. *International Geophysics Series*, *46*, 9–11.

Phillips, H. E., & Rintoul, S. R. (2000). Eddy variability and energetics from direct current measurements in the Antarctic Circumpolar Current south of Australia. *Journal of Physical Oceanography*, *30*(12), 3050–3076. (https://doi.org/10.1175/1520-0485(2000)030<3050:EVAEFD>2.0.CO;2)

Pickart, R. S., & Huang, R. X. (1995). Structure of an inertial deep western boundary current. *Journal of marine research*, *53*(5), 739–770. (https://doi.org/10.1357/0022240953213007)

Pond, S., & Pickard, G. L. (2013). *Introductory dynamical oceanography*. Elsevier.

Pratt, L. L., & Whitehead, J. A. (2007). *Rotating Hydraulics: Nonlinear Topographic Effects in the Ocean and Atmosphere* (Vol. 36). Springer Science & Business Media. (http://doi.org/10.1007/978-0-387-49572-9)

Rhein, M., Stramma, L., & Send, U. (1995). The Atlantic Deep Western Boundary Current: Water masses and transports near the equator. *Journal of Geophysical Research: Oceans*, *100*(C2), 2441–2457. (https://doi.org/10.1029/94JC02355)

Rhines, P. B., & Holland, W. R. (1979). A theoretical discussion of eddy-driven mean flows. *Dynamics of Atmospheres and Oceans*, *3*(2-4), 289–325. (https://doi.org/10.1016/0377-0265(79)90015-0)

Rintoul, S. R. (1991). South Atlantic interbasin exchange. *Journal of Geophysical Research: Oceans*, *96*(C2), 2675–2692. (https://doi.org/10.1029/90JC02422)

Røed, L. P. (1980). Curvature effects on hydraulically driven inertial boundary currents. *Journal of Fluid Mechanics*, *96*(2), 395–412. (`https://doi.org/10.1017/S0022112080002182`)

Schott, F. A., Brandt, P., Hamann, M., Fischer, J., & Stramma, L. (2002). On the boundary flow off Brazil at 5–10 °S and its connection to the interior tropical Atlantic. *Geophysical Research Letters*, *29*(17). (`https://doi.org/10.1029/2002GL014786`)

Schott, F. A., Dengler, M., Zantopp, R., Stramma, L., Fischer, J., & Brandt, P. (2005). The shallow and Deep Western Boundary Circulation of the South Atlantic at 5–11°S. *Journal of Physical Oceanography*, *35*(11), 2031–2053. (`https://doi.org/10.1175/JPO2813.1`)

Schulzki, T., Getzlaff, K., & Biastoch, A. (2021). On the Variability of the DWBC Transport Between 26.5N and 16N in an Eddy-Rich Ocean Model. *Journal of Geophysical Research: Oceans*, *126*(6), Art–Nr. (`https://doi.org/10.1029/2021JC017372`)

Silveira, I. C. A., Brown, W. S., & Flierl, G. R. (2000). Dynamics of the North Brazil Current retroflection region from the Western Tropical Atlantic Experiment observations. *Journal of Geophysical Research: Oceans*, *105*(C12), 28559–28583.

Silveira, I. C. A., de Miranda, L. B., & Brown, W. S. (1994). On the origins of the North Brazil Current. *Journal of Geophysical Research: Oceans*, *99*(C11), 22501–22512. (`https://doi.org/10.1029/94JC01776`)

Silveira, I. C. A., Lima, J. A. M., Schmidt, A. C. K., Ceccopieri, W., Sartori, A., Franscisco, C. P. F., & Fontes, R. F. C. (2008). Is the meander growth in the Brazil Current system off Southeast Brazil due to baroclinic instability? *Dynamics of Atmospheres and Oceans*, *45*(3-4), 187–207. (`https://doi.org/10.1016/j.dynatmoce.2008.01.002`)

Solodoch, A., McWilliams, J. C., Stewart, A. L., Gula, J., & Renault, L. (2020). Why Does the Deep Western Boundary Current "Leak" around Flemish Cap? *Journal of Physical Oceanography*, *50*(7), 1989–2016. (`https://doi.org/10.1175/JPO-D-19-0247.1`)

Spingys, C. P., Naveira Garabato, A. C., Legg, S., Polzin, K. L., Abrahamsen, E. P., Buckingham, C. E., . . . Frajka-Williams, E. E. (2021). Mixing and Transformation in a Deep Western Boundary Current: A Case Study. *Journal of Physical Oceanography*, *51*(4), 1205–1222. (`https://doi.org/10.1175/JPO-D-20-0132.1`)

Stern, M. E., & Whitehead, J. A. (1990). Separation of a boundary jet in a rotating fluid. *Journal of Fluid Mechanics*, *217*, 41–69. (`https://doi.org/10.1017/S0022112090000623`)

Stramma, L., Fischer, J., & Reppin, J. (1995). The North Brazil Undercurrent. *Deep Sea Research Part I: Oceanographic Research Papers*, *42*(5), 773–795. (`https://doi.org/10.1016/0967-0637(95)00014-W`)

Talley, L. D., Pickard, G. L., Emery, W. J., & Swift, J. H. (2011). *Descriptive Physical Oceanography: An Introduction*. Academic Press. (`https://doi.org/10.1016/C2009-0-24322-4`)

Tomczak, M., & Godfrey, J. S. (1994). Regional oceanography: An introduction. *Elsevier Science ltd*, *660*, 10591–5153.

Torrence, C., & Compo, G. P. (1998). A practical guide to wavelet analysis. *Bulletin of the American Meteorological society*, *79*(1), 61–78. (https://doi.org/10.1175/1520-0477(1998)079<0061:APGTWA>2.0.CO;2)

Trott, C. B., Subrahmanyam, B., Chaigneau, A., & Delcroix, T. (2018). Eddy tracking in the northwestern Indian Ocean during southwest monsoon regimes. *Geophysical Research Letters*, *45*(13), 6594–6603.

Vallis, G. K. (2017). *Atmospheric and Oceanic Fluid Dynamics*. Cambridge University Press. (`https://doi.org/10.1017/9781107588417`)

van Sebille, E., Johns, W. E., & Beal, L. M. (2012). Does the vorticity flux from Agulhas rings control the zonal pathway of NADW across the South Atlantic? *Journal of Geophysical Research: Oceans*, *117*(C5). (`https://doi.org/10.1029/2011JC007684`)